

1 **Size distribution and optical properties of mineral dust**
2 **aerosols transported in the western Mediterranean**

3

4C. Denjean^{1,2}, F. Cassola³, A. Mazzino³, S. Triquet¹, S. Chevaillier¹, N. Grand¹, T. Bourriane⁴,
5G. Momboisse⁴, K. Sellegri⁵, A. Schwarzenbock⁵, E. Freney⁵, M. Mallet⁶ and P. Formenti¹

6

7[1] Laboratoire Interuniversitaire des Systèmes Atmosphériques (LISA), UMR-CNRS 7583,
8Université Paris-Est-Créteil (UPEC) et Université Paris Diderot (UPD), Institut Pierre Simon
9Laplace (IPSL), Créteil, France

10[2] Leibniz Institute for Tropospheric Research (TROPOS), Permoserstraße 15, 04318,
11Leipzig, Germany

12[3] Department of Physics and INFN, Genoa, Italy

13[4] Centre National de Recherches Météorologiques (CNRM), Météo-France, Toulouse,
14France

15[5] Laboratoire de Météorologie Physique (LaMP), CNRS/Université Blaise Pascal,
16Clermont-Ferrand, France

17[6] Laboratoire d'Aérodynamique (LA), Université de Toulouse, CNRS, Toulouse, France

18

19Correspondance to : Cyrielle Denjean (cyrielle.denjean@meteo.fr), Paola Formenti
20(paola.formenti@lisa.u-pec.fr)

21

1 Abstract

2 This study presents *in situ* aircraft measurements of Saharan mineral dust transported over the
3 western Mediterranean basin in June-July 2013 during the ChArMEx/ADRIMED (the
4 Chemistry-Aerosol Mediterranean Experiment / Aerosol Direct Radiative Impact on the
5 regional climate in the MEDiterranean region) airborne campaign. Dust events differing in
6 terms of source region (Algeria, Tunisia and Morocco), time of transport (1-5 days) and height
7 of transport were sampled. Mineral dust were transported above the marine boundary layer,
8 which conversely was dominated by pollution and marine aerosols. The dust vertical structure
9 was extremely variable and characterized by either a single layer or a more complex and
10 stratified structure with layers originating from different source regions. Mixing of mineral
11 dust with pollution particles was observed depending on the height of transport of the dust
12 layers. Dust layers carried higher concentration of pollution particles below 3 km above sea
13 level (asl.) than above 3 km asl., resulting in scattering Ångstrom exponent up to 2.2 below 3
14 km asl.. However, the optical properties of the dust plumes remained practically unchanged
15 with respect to values previously measured over source regions, regardless of the altitude.
16 Moderate absorption of light by the dust plumes was observed with values of aerosol single
17 scattering albedo at 530 nm ranging from 0.90 to 1.00. Concurrent calculations from the
18 aerosol chemical composition revealed a negligible contribution of pollution particles to the
19 absorption properties of the dust plumes that was due to a low contribution of refractory black
20 carbon in regards to the fraction of dust and sulfate particles. This suggests that, even in the
21 presence of moderate pollution, likely a persistent feature in the Mediterranean, the optical
22 properties of the dust plumes could be assumed similar to those of native dust in radiative
23 transfer simulations, modeling studies and satellite retrievals over the Mediterranean.
24 Measurements also showed that the coarse mode of mineral dust was conserved even after 5
25 days of transport in the Mediterranean, which contrasts with the gravitational depletion of
26 large particles observed during the transport of dust plumes over the Atlantic. Simulations
27 with the WRF mesoscale meteorological model highlighted a strong vertical turbulence within
28 the dust layers that could prevent deposition of large particles during their atmospheric
29 transport. This has important implications for the dust radiative effects due to surface
30 dimming, atmospheric heating and cloud formation. The results presented here add to the
31 observational dataset necessary for evaluating the role of mineral dust on the regional climate
32 and rainfall patterns in the western Mediterranean basin and understanding their atmospheric
33 transport at global scale.

34

1
2

11. Introduction

2 Mineral dust aerosols constitute a major fraction of airborne particulate matter (Huneeus et al., 2012) and their contribution to the Earth's climate system is of considerable significance. 4 In particular, dust aerosols exert a significant effect on global radiative budget by scattering 5 and absorbing longwave and shortwave radiation (IPCC, 2013), thereby impacting the vertical 6 profile of temperature and atmospheric stability (Jing et al., 2008) and the precipitation rate 7 (Rosenfeld et al., 2001; Andreae and Rosenfeld, 2008; Choobari et al., 2014).

8 The Sahara desert hosts the maximum dust emission and atmospheric dust loading in the 9 world (Choobari et al., 2014). Strong winds and convection produced by intense surface 10 heating can uplift mineral dust particles into the free troposphere, where they are advected 11 over large distances at the continental and intercontinental scales (d'Almeida, 1986; Goudie 12 and Middleton, 2001; Engelstaedter et al., 2006). Along the year, the transport pathway of 13 Saharan dust is mainly controlled by low-pressure systems over the Atlantic or North Africa, 14 high pressure over the Mediterranean region, or high pressure at upper level over Africa 15 (Moulin et al., 1998; Querol et al., 2009; Salvador et al., 2014). A significant fraction of dust 16 loaded from Africa sources are transported westward across the Atlantic Ocean as far as the 17 Caribbean (Maring et al., 2003; Doherty et al., 2008), the United States (Perry et al., 1997; 18 Prospero et al., 2002) and South America (Swap et al., 1992; Formenti et al., 2001; Ansmann 19 et al., 2009). Large Saharan dust storms are also carried across the Mediterranean Sea to 20 Europe (Moulin et al., 1998; Koren et al., 2003; Collaud Coen et al., 2004; Van Dingenen et 21 al., 2005; Papayannis et al., 2008). During such outbreaks, mineral dust emerges as the largest 22 PM_{10} source at rural and urban sites in the Mediterranean basin (Pey et al., 2013; Salvador et 23 al., 2014).

24 Considerable uncertainties in quantifying the climatic effect of mineral dust arise from a lack 25 of knowledge of their properties and spatial and vertical distributions over many regions of 26 the world. In particular, to estimate the magnitude of the dust radiative effect, an accurate 27 description of both particle size distribution and optical properties and their link with the 28 chemical composition is necessary (Sokolik and Toon, 1996; Tegen et al., 1996). The size 29 distribution is a fundamental parameter to estimate the aerosol radiative effect and 30 atmospheric lifetime, but its representation remains challenging due to the large size spectrum 31 of mineral dust, from hundreds of nanometers to tens of micrometers (Formenti et al., 2011a). 32 In particular, an accurate description of the coarse mode particles is vital since the presence of 33 large particles enhances the capacity of mineral dust in absorbing radiation at short and long 34 wavelengths (McConnell et al., 2008; Otto et al., 2009; Sicard et al., 2014), modifies the

1atmospheric heating rate (Ryder et al., 2013a) and affects cloud formation (Koehler et al., 22009).

3Once in the atmosphere, mineral dust can undergo various aging processes, such as
4heterogeneous reactions with gas-phase compounds (Sullivan and Weber, 2006; Ma et al.,
52012), condensation of low-volatile species (Bauer et al., 2004; Clarke et al., 2004; Sullivan
6and Prather, 2007), cloud processing (Levin et al., 1996; Trochkin et al., 2003) and
7coagulation (Fan et al., 1996; Zhou et al., 1996; Levin et al., 2005). Because of these
8processes, the physico-chemical properties (composition, mixing state, shape, and size
9distribution) of dust aerosols might evolve during transport, leading in turn to the evolution of
10the optical properties (Formenti et al., 2011a). A recent study of Kanitz et al. (2014) has
11shown significant differences in the optical properties of two Saharan dust plumes over the
12Atlantic Ocean, resulting from different aging processes affecting the dust. Henceforth, the
13radiative effect of mineral dust should depend on the travel distance and pathway, residence
14time over their source regions and air masses encountered (Garrett et al., 2003).

15The Mediterranean basin provides ideal conditions to investigate the changes in Saharan dust
16properties as numerous concurrent anthropogenic and natural sources of aerosols are active
17over this region. Case studies of mixing of Saharan dust with industrial/urban, marine and
18biomass burning particles have been documented in the past (Koçak et al., 2012; Mantas et
19al., 2014), and could explain the large variability of the values of single scattering albedo ω_0
20(0.83-0.92 at the wavelength of 440 nm) reported by various studies (Sicard et al., 2012;
21Mallet et al., 2013).

22In past years, intensive field campaigns including *in situ* airborne measurements have mostly
23focused on properties of mineral dust at emission (e.g., over the Saharan and the Sahelian
24source regions) and over the Atlantic Ocean, and their comparison to trace the temporal
25evolution during transport (Formenti et al., 2003, 2011b; Reid et al., 2003; McConnell et al.,
262008; Osborne et al., 2008; Heintzenberg, 2009; Weinzierl et al., 2009, 2011; Haywood et al.,
272011; Ryder et al., 2013a,b). On the contrary, observations in the Mediterranean region were
28mostly limited to remote sensing from the ground (e.g. Hamonou et al., 1999; Meloni et al.,
292006; Saha et al., 2008; Basart et al., 2009; Gómez-Amo et al., 2011; Perrone and Bergamo,
302011; Mallet et al., 2013; Pey et al., 2013; Marconi et al., 2014) or spaceborne (Moulin et al.,
311997; de Meij and Lelieveld, 2011; Gkikas et al., 2012).

32To fill this gap, the Aerosol Direct Radiative Impact on the regional climate in the
33MEDiterranean region (ADRIMED) field campaign, part of the international cooperative
34research program ChArMEx (the Chemistry-Aerosol Mediterranean Experiment;

1 <http://charmex.lsce.ipsl.fr>) took place with the main objectives of characterizing Saharan dust
2 plumes by coordinated aircraft and ground-based measurements (Mallet et al., 2015). In this
3 paper, we present *in situ* aircraft measurements obtained in June-July 2013 over the
4 Mediterranean basin. The objective is to determine possible changes of dust properties during
5 long-range transport over the western Mediterranean basin and explore the potential reasons
6 for changes.

7 Section 2 describes the aircraft strategy, the instrumentation and the method used to determine
8 the aerosol size distribution, chemical composition and the associated optical properties.
9 Section 3 presents the campaign meteorology, the dust vertical profiles and the results of the
10 aerosol properties within the dust plumes. Section 4 explores the potential factors affecting the
11 variability of the aerosol properties due to altitude and dust age. Section 5 concludes this
12 article.

13

14 **2. Measurement and methodology**

15 **2.1. Aircraft strategy**

16 The ATR-42 aircraft of SAFIRE (French aircraft service for environmental research,
17 <http://www.safire.fr>) based at Cagliari (39°15'N, 9°03'E, Italy) conducted 16 flights in the
18 period 14 June - 04 July 2013. In this paper, we present results from the 9 flights dedicated to
19 the observation of mineral dust plumes that occurred between 16 June and 03 July 2013.
20 These flights were carefully selected to provide measurements of air masses from dust active
21 sources based on the analysis of satellite images and backward trajectories, as described in
22 section 2.4.

23 The ATR-42 aircraft performed research flights in the area between 35° - 43° N and -4° - 13° E
24 covering the western Mediterranean region to probe the Saharan dust properties in a range of
25 varying transport pathways and source regions. The flight tracks are shown in Figure 1 and a
26 summary of flight information is provided in Table 1.

27 The airborne missions were planned using four different dust plume forecast models (MACC
28 ALADIN-Dust, SKIRON and BSC-DREAM8b v2.0) and satellite images from the SEVIRI
29 radiometer on the Meteosat Second Generation (MSG) satellite, all available in real time from
30 the ChArMex Operating Center (<http://choc.sedoo.fr/>) during the campaign. A general
31 weather forecast was made daily by the French school of Meteorology (ENM), at Météo-
32 France in Toulouse.

33 The general flight strategy consisted of two main parts: first, profiles from 300 m up to 6 km
34 above sea level (asl) were conducted by performing a spiral trajectory 10-20 km wide to

1 sound the vertical structure of the atmosphere and identify interesting dust layers. Afterwards,
2 the identified dust layers were probed by straight levelled runs (SLR), where the aircraft flew
3 at fixed altitudes, to provide information on dust spatial variability and properties. Horizontal
4 flight legs in the dust layers lasted 20-40 min to allow aerosol collection on filters for
5 chemical analyses in the laboratory. At the typical aircraft cruise speed of 100 m s^{-1} , samples
6 had spatial resolution ranging from 121 to 242 km.

7

8 **2.2. Instrumentation**

9 The ATR-42 basic instrumentation provides meteorological parameters including temperature,
10 dew point temperature, pressure, turbulence, relative humidity, wind speed, direction, CO and
11 O_3 concentrations (Saïd et al., 2010). Only instruments relevant to microphysical properties,
12 chemical composition and optical properties of aerosols are detailed in Table 2.

13

14 **2.2.1. Aerosol concentration and size distribution**

15 The total number concentration of particles larger than 5 nm in diameter was measured using
16 a butanol-based condensation nucleus counter (CPC, TSI model 3075) corrected for
17 coincidences.

18 The particle number size distribution was measured over the largest possible size spectrum by
19 combining optical and electrical mobility techniques. The number size distribution in the
20 submicron range was measured with an in-cabin Scanning Mobility Particle Sizer (SMPS)
21 and a wing-mounted Ultra High Sensitivity Aerosol Spectrometer (UHSAS, Droplet
22 Measurement Technologies). The SMPS consisted of a Differential Mobility Analyzer (DMA,
23 Villani et al., 2007) interfaced to a Condensation Particle Counter (CPC, TSI model 3010). A
24 closed-loop recirculation was used for the sheath flow of the DMA. The SMPS system
25 provided the number size distribution of the electrical mobility diameter from the 30 - 400 nm
26 in 135 nominal size classes (i.e. size classes provided by the instrument not corrected for the
27 dynamic shape factor) over time scans lasting 120 seconds. Therefore, only data acquired
28 during SLR are considered. Data were processed by taking into account the particle electrical
29 charging probabilities, the CPC counting efficiencies, the DMA transfer functions and the
30 diffusion losses in the SMPS and CPC systems. The UHSAS is an optical-scattering laser-
31 based aerosol spectrometer, providing the number size distribution of the optical equivalent
32 diameter from 0.04 to $1 \mu\text{m}$ in 99 nominal size classes at a time resolution of 1 second. The
33 spectrometer integrates light scattering between 22 to 158° at 1054 nm. Due to reduced
34 counting efficiency at size larger than $0.9 \mu\text{m}$, only data at lower sizes are considered in this

1

2

1paper. The uncertainties on the particle diameter were estimated to be 5% and 10% for the
2SMPS and UHSAS, respectively (Wiedensohler et al., 2012; Cai et al., 2008).

3The number size distribution in the supermicron range was measured by the combination of
4two different optical particle counters (OPC). A wing-mounted Forward Scattering
5Spectrometer Probe (FSSP, Particle Measuring System, Model 300) measured the optical size
6distribution in the nominal size range of 0.28 to 20 μm (Baumgardner et al., 1992). Data were
7recorded in 30 size classes at 1 second interval. The FSSP-300 is based on the measurement
8of the light scattered between 3 and 12° at 632.8 nm. The FSSP has an uncertainty in diameter
9of about 30% according to Baumgardner et al. (1992). A GRIMM OPC (model sky-OPC
101.129) operated inside the cabin at a 6-second time resolution for measuring the optical size
11distributions between 0.3 and 32 μm on 32 size classes in nominal diameter. However, only
12data at nominal size below 12 μm were considered here due to the passing efficiency of the
13aerosols inlets connected to the GRIMM (see section 2.3.2. for further information). The
14instrument integrates light scattering between 30 and 150° at 655 nm. According to the
15calibration of the GRIMM with size-standard particles, we assumed an uncertainty in
16diameter of 10%.

17

182.2.2. Aerosol chemical composition

19Bulk aerosol samples were collected on-board by filtration through two stainless-steel filter
20units mounted in parallel. Sampling was performed only during constant altitude sequences
21lasting more than 25 minutes in order to guarantee sufficient mass loading of the filter
22samples. After exposure, samples were stored and transported at -20°C to avoid later
23modification. Once in the laboratory, samples collected on 42-mm diameter polycarbonate
24membranes (nominal pore size 0.4 μm Nuclepore, Whatman) were cut in halves that were
25analyzed to yield both the elemental and ionic composition. Concentrations of elements from
26Na to Pb were measured by wavelength-dispersive X-ray fluorescence (WD-XRF) using a
27PW-2404 spectrometer (Panalytical). Details of the analytical protocols are provided by
28Formenti et al. (2008). The concentration of water-soluble ions were determined by Ion
29chromatography (IC) with a Metrohm IC 850 device equipped with an injection loop of 100
30 μl . For anionic species, IC has been equipped with Metrosep A supp 16 (250/4.0mm) column
31associated with a metrosepA supp 16 guard pre-column heated at 65°C. For simultaneous
32separation of inorganic and short-chain organic anions, elution has been realized with eluant
33composed at 20% by ultrapure water and at 80% by a solution 7.5 mM Na_2CO_3 and 0.75mM
34NaOH. The elution flow rate was 0.8 mL min^{-1} . For cationic species, IC has been equipped

1

2

1with a Metrosep C4 (250/4.0mm) column associated to a metrosep C4 guard column heated at
230°C. Elution has been realized with an eluant composed with 0.7 mM of dipicolinic acid and
31.7 mM of nitric acid. The elution flow rate was 1 mL min⁻¹.

4The mass concentration of refractory black carbon particles (rBC) was measured using a
5single particle soot photometer (SP2, DMT). The SP2 uses a continuous intra-cavity Nd:YAG
6laser at the wavelength of 1064 nm to heat rBC-containing particles to their vaporization
7point. Single particle rBC mass was derived from the peak intensity of the thermal radiation
8emitted by the incandescent rBC detected by the SP2. This method allows the quantification
9with 100% efficiency of rBC mass in single particles with mass equivalent diameters between
1080-500 nm (Moteki and Kondo, 2010). The total rBC mass loading was reported as the sum of
11all the detected single particle rBC masses. Prior to the measurement field campaign, the SP2
12was calibrated using fullerene soot particles, which have been shown to give similar SP2
13response as ambient rBC (Moteki and Kondo, 2010; Baumgardner et al., 2012; Laborde et al.,
142012).

15

162.2.3. Aerosol scattering and extinction coefficients

17The particle scattering coefficient (σ_{scat}) was measured at three wavelengths (450, 550 and 700
18nm) with an integrating nephelometer (TSI, model 3563), which integrates light scattered by
19particles at scattering angle between 7° and 170° relative to the incident and scattered
20radiation. The instrument operated at a volumetric flow rate of 30 L min⁻¹ and the data were
21acquired at 1-s time resolution. The instrument was calibrated with free-particle air and high-
22purity CO₂ prior to and after the campaign. Uncertainty in σ_{scat} measured with the
23nephelometer is estimated to be 5% (Muller et al., 2011a). Measured values were corrected for
24the angular truncature error in the nephelometer measurements at angles smaller than 7° and
25greater than 170° as described in section 2.3.2.

26The particle extinction coefficient (σ_{ext}) was measured with a Cavity Attenuated Phase Shift
27particle light extinction monitor (CAPS-PMex, Aerodyne Research) operated at the
28wavelength of 530 nm. The instrument relies on measuring the average time spent by the light
29within the sample cell that has an optical path length of 1-2 km. The sampling volumetric
30flowrate was 0.85 L min⁻¹ and data were processed with a time resolution of 1 second.
31Uncertainty in σ_{ext} measured with the CAPS is estimated to be 3% (Massoli et al., 2010).

32

33

34

1

2

12.3. Aerosol data analysis

2Figure 2 depicts the iterative procedure used to retrieve the aerosol size distribution and
3optical parameters relevant to this paper. We focused our attention on aerosol parameters used
4in climate models for calculating the direct and semi-direct aerosol radiative effects:

5- The complex refractive index \tilde{n} defined as $n_r - in_i$, where n_r and n_i are the real and imaginary
6part representing the particle scattering and absorption properties, respectively.

7- The single scattering albedo ω_0 (unitless) representing the balance between the scattering and
8the absorbing properties and defined as:

9

$$\omega_0(\lambda) = \frac{\sigma_{scat}(\lambda)}{\sigma_{ext}(\lambda)} \quad (1)$$

10(where σ_{scat} is the aerosol scattering coefficient (expressed in $Mm^{-1} = 10^{-6} m^{-1}$), σ_{ext} the aerosol
11extinction coefficient (Mm^{-1}) and λ the wavelength (nm).

12- The asymmetry parameter g (unitless) describing the angular distribution of the scattered
13radiation and defined as:

$$g(\lambda) = \frac{1}{2} \int_0^\pi \cos(\Theta) \sin(\Theta) P(\Theta, \lambda) d\Theta \quad (2)$$

14where $P(\Theta, \lambda)$ is the scattering phase function and Θ is the scattering angle.

15- The mass extinction efficiency k_{ext} ($m^2 g^{-1}$) representing the total light extinction per unit
16mass concentration of aerosol and calculated as:

$$k_{ext}(\lambda) = \frac{\sigma_{ext}(\lambda)}{C_m} \quad (3)$$

17where C_m is the aerosol mass concentration ($\mu g m^{-3}$).

18In this study, we have decided to neglect the non-sphericity of mineral dust since the sphere
19model has been shown to produce negligible errors when computing radiative fluxes and flux
20related quantities, i.e. aerosol optical depth (AOD), ω_0 and g (Mishchenko et al., 1995).
21Because we only investigate angular-integrated properties and for sake of comparison with the
22large majority of field data published so far, in this paper we only perform calculations in the
23spherical approximation.

24

25

26

27

1

2

12.3.1. Assessment of aerosol size distributions

2The particle size distribution was derived from the SMPS, UHSAS, GRIMM and FSSP-300.
3For size distributions measured by SMPS, the electrical mobility D_m and the geometric
4particle diameters D_g are related by the dynamic shape factor (DeCarlo et al., 2004):

$$D_g = \frac{D_m}{\chi} \quad (4)$$

5The dynamic shape factor χ depends on the shape of the particles (Hinds, 1999). In this study,
6we have decided to neglect the non-sphericity of mineral dust to maintain retrieval conditions
7similar to those of previous literature studies on dust in source region. Henceforth, χ was set to
8unity.

9Optical sizing instruments (i.e. UHSAS, GRIMM, FSSP-300) measure the amount of light
10scattered by a single particle and convert this into a geometric particle size. This conversion
11depends on the complex refractive index of the aerosol, as well as on the optical geometry and
12the laser wavelength of the instrument. The correction procedure used the Mie scattering
13theory for homogeneous spheres with known complex refractive index (Bohren and Huffman,
141983).

15As discussed by Reid et al. (2003), the conversion of scattered light into particle size can lead
16to ambiguity in the sizing of the coarse mode diameters. If the light intensity response of the
17optical sizing instruments is non-unique it can lead to oversizing of larger particles. This
18happens mostly for forward scattering probes, such as the FSSP-300, as demonstrated in
19Figure S1 showing a flattening in the scattering cross section curves integrated over the FSSP-
20300 scattering angle range (3-15°) between 2 and 10 μm diameter. For the GRIMM 1.129
21scattering angles (30-150°), the scattering cross section is unique with size, except between
221.5-2 μm where an inflection point can be seen. During ADRIMED, systematic differences in
23the size distributions measured by the FSSP-300 and the GRIMM were observed around 2
24 μm . Given the response curves in Figure S1, data between 2-10 μm and 1.5-2 μm diameter
25from the FSSP-300 and the GRIMM, respectively, were not considered in this paper.

26Figure 3 presents an example of size distributions measured in a dust plume by the different
27instruments. As will be discussed below, the value of $\tilde{n} = 1.53 - 0.004i$ at 530 nm was the most
28appropriate to reconstitute both scattering and extinction coefficient and therefore we present
29results using this value in Figure 3. Overall, the comparison between different instruments
30shows good consistency, giving credence to the measurements and the choice of refractive
31index and dynamic shape factor.

1The resulting number and volume size distributions were parameterized by fitting four log-
2normal distributions, as:

$$\frac{dN}{d\log D_p} = \sum_{i=1}^4 \frac{N_{tot,i}}{\sqrt{2\pi} \cdot \log \sigma_i} \exp \left[-\frac{(\log D_p - \log D_{p,g,i})^2}{2(\log \sigma_i)^2} \right] \quad (5)$$

$$\frac{dV}{d\log D_p} = \sum_{i=1}^4 \frac{N_{tot,i} \cdot \frac{\pi}{6} \cdot D_p^3}{\sqrt{2\pi} \cdot \log \sigma_i} \exp \left[-\frac{(\log D_p - \log D_{p,g,i})^2}{2(\log \sigma_i)^2} \right] \quad (6)$$

3each mode i being characterized by characterized by the integrated number concentration $N_{tot,i}$,
4the geometric median diameter $D_{p,g,i}$ and the geometric standard deviation σ_i (i.e. Figure 3).

5To provide a synthetic representation of the particle number size distributions, the effective
6particle D_{eff} was calculated as :

$$D_{eff} = \frac{\int D_p^3 \frac{dN}{dD_p} dD_p}{\int D_p^2 \frac{dN}{dD_p} dD_p} \quad (7)$$

7 D_{eff} has been estimated separately on the fine and coarse fractions in the size ranges 0.053-1
8 μm (referred as $D_{eff,f}$ thereafter) and 1-20 μm (referred as $D_{eff,c}$), respectively.

9

102.3.2. Assessment of aerosol optical properties

11An iterative procedure was used to derive \tilde{n} , ω_0 , g and k_{ext} at 530 nm and correct σ_{scat} for the
12angular truncature error (i.e. Figure 2). The parametrized size distributions were used as input
13for the Mie scattering calculations (Bohren and Huffman, 1983), which were done by varying
14stepwise the real part of the complex refractive index n_r from 1.33 to 1.60 and the imaginary
15part of the complex refractive index n_i from 0.000 to 0.020. \tilde{n} was assumed to be constant with
16particle size and have thus to be regarded as an effective value for the entire particle
17population. σ_{scat} was adjusted to the CAPS operation wavelength of 530 nm by using the
18following equation:

19

$$\mathring{A}(\lambda_1, \lambda_2) = -\frac{\ln(\sigma_{scat}(\lambda_1)/\sigma_{scat}(\lambda_2))}{\ln(\lambda_1/\lambda_2)} \quad (8)$$

20where \mathring{A} represents the spectral dependence of the scattering coefficient and λ_1 and λ_2 are the
21wavelength interval. \mathring{A} is often used as a qualitative indicator of aerosol particle size or fine
22mode fraction (Seinfeld and Pandis, 1998). Typically, it is lower than ~ 0.5 for aerosols

1
2

1 dominated by coarse particles, such as mineral dust or sea salt, but it is higher than 1 for fine
2 particles, such as pollution particles or biomass burning. The calculated values of $\sigma_{scat}(530nm)$
3 and $\sigma_{ext}(530nm)$ were compared to that measured by the nephelometer and the CAPS, and
4 values having the closest agreement within the measurement error bars were chosen as the
5 best estimate.

6 The in-aircraft aerosol instruments sampled through isokinetic and isoaxial aerosol inlets. The
7 nephelometer and GRIMM were set up behind the AVIRAD inlet, while the CAPS, SMPS and
8 SP2 were set up behind the Community Aerosol Inlet (CAI). Particle loss can occur both as a
9 result of the inlet aspiration efficiency and the transport losses in the pipework between the
10 inlet and the instruments. The cut-off diameter, at which the passing efficiency of the inlet
11 equals 50%, was determined by a set of wind-tunnel experiments (unpublished data). The
12 passing efficiency was determined as the ratio of the particle number concentration measured
13 by GRIMM optical counters behind the sampling lines of the AVIRAD and CAI inlets to the
14 particle number concentration measured in the main flow of the wing tunnel where the air
15 speed was 93 m s^{-1} as the cruise speed of the ATR-42. Monodisperse polystyrene latex spheres
16 of 0.6, 1.2, 4.6, 7.9 and $11 \mu\text{m}$ diameter (Duke Scientifics, Thermo Sci.) and polystyrene
17 divinylbenzene spheres of diameter varying between 1 and $35 \mu\text{m}$ in diameter (also purchased
18 from Duke Scientifics) were first diluted and then put in a reservoir connected to a peristaltic
19 pump. The pump tubing was connected to a pneumatic spinning disk (SPIDI) in order to spray
20 a large amount of droplets from the solution, some droplets having a particle incorporated. An
21 air mover was mounted beneath the SPIDI and thus the droplets were rapidly evaporated. The
22 particle size-dependent passing efficiency of the AVIRAD and CAI sampling inlets shown in
23 Figure S2 indicates that the cut-off diameter value, expressed as optical equivalent, is $12 \mu\text{m}$
24 for the AVIRAD inlet and $5 \mu\text{m}$ for the CAI.

25 To assess the impact of the inlets sampling efficiency on the measured optical properties, Mie
26 scattering calculations were performed to estimate n_r , n_i , ω_0 , g and k_{ext} using either the full
27 size distribution or the size distribution measured behind the aircraft inlets. For ω_0 , g and k_{ext} ,
28 we considered a fixed refractive index of $1.52-0.003i$, reflective of the values observed for
29 Saharan dust in source region (Schladitz et al., 2009; Formenti et al., 2011a; Ryder et al.,
30 2013a). The discrepancies between ω_0 , g and k_{ext} , including or not larger particle sizes were
31 used to estimate the errors associated to the inlets sampling efficiency. For n_r and n_i , we
32 estimated the difference between \tilde{n} derived from the iterative procedure described above (i.e.
33 Fig. 2) using the full size distribution as input parameter and that obtained from the size
34 distribution measured behind the aircraft inlets. The absolute errors associated with ω_0 , g and

1 k_{ext} due to the passing efficiencies of the inlets were estimated to be 0.02, 0.002, 0.04, 0.05
2 and 0.08, respectively, which is in the range covered by the measurements uncertainties of
3 both optical parameters and size distributions..

4

52.4. Ancillary products

6 Weather Research and Forecasting (WRF; Skamarock et al. 2008) simulations were
7 performed to investigate the meteorological conditions and the turbulence within the dust
8 layers. The WRF model is operational at the Department of Physics of the University of
9 Genoa, Italy, in a three-domain configuration. In particular, the simulations on the parent
10 domain, covering the entire Mediterranean basin with a horizontal grid spacing of 10 km,
11 have been considered for the present paper. Initial and boundary conditions were generated
12 from the operational global model GFS (Environmental Modeling Center, 2003) outputs (0.5
13 \times 0.5 square degree). More details about the modelling chain and the model setup are given in
14 Bove et al. (2014), Cassola et al. (2015), and Mentaschi et al. (2015).

15 As a complement, synoptic conditions and sea level pressure composite anomalies over the
16 Mediterranean basin during the campaign were analyzed using reanalysis data sets, such as
17 the NCEP/NCAR Reanalysis (Kalnay et al. 1996) and the NCEP Climate Forecast System
18 (CFS) reanalysis (Saha et al., 2010).

19 Source regions and atmospheric transport times of the dust plumes were determined through
20 the combination of satellite products and backward trajectories analysis. The potential source
21 regions active during the observational period were identified using the images from the
22 Spinning Enhanced Visible and Infrared Imager (SEVIRI) onboard the Meteosat Second
23 Generation (MSG) satellite. The NOAA Hybrid Single-Particle Lagrangian Integrated
24 Trajectory Model (HYSPLIT, <http://www.arl.noaa.gov/HYSPLIT.php>) using the Global Data
25 Assimilation System (GDAS) meteorological input was used to calculate whether an air mass
26 sampled by the aircraft could have originated from one of the identified active dust sources.
27 Backward trajectories were initialized using the time and the location when the aircraft
28 intercepted the air mass and were extended for up to 5 days prior the measurement. Backward
29 trajectory calculations were performed at the beginning, the middle and at the end of each
30 SLR to check the origin and transport pathway of the air masses sampled by the aircraft
31 through the measurements. We then operationally define the dust age as the time elapsed since
32 the calculated air mass trajectory leave the ground where an active source was detected and up
33 to the time of sampling by the aircraft.

34

1
2

13. Results

23.1. Identification of the dust source region and transport pathway

3 During the ChArMEx/ADRI-MED campaign, the synoptic situation was characterized by a
4 “dipolar” sea level pressure anomaly pattern, with positive anomalies in the western
5 Mediterranean and negative ones in the eastern part of the basin, as illustrated in Figure 4 (left
6 panel). While this situation induced stronger and more frequent than normal northwesterly
7 winds over the Sardinia and Sicily channels, the average conditions at mid-atmospheric levels
8 during the campaign were closer to climatological ones (Figure 4, right panel). Moulin et al.
9 (1998) have documented the frequency of dust episodes across the Mediterranean Sea,
10 summer occurrences are quite frequent.

11 The synoptic conditions during each of the 9 flights described in Figure 1 and Table 1 are
12 summarized in Figure S3 and S4 in the Supplementary Material, where sea level pressure and
13 500-hPa geopotential height are shown. A low-pressure system can be found over the Atlantic
14 on June 16, moving towards the Iberian Peninsula, while a subtropical ridge extends from
15 North Africa to central Mediterranean. This situation induced a strong south-southwesterly
16 flow, firstly towards southern Iberia and western Mediterranean (16-17 June), then extending
17 eastwards and reaching Corsica on the subsequent days, favouring dust transport from the
18 Saharan region. This is quite evident from Figure S5, showing 700-hPa wind and relative
19 humidity maps from the WRF model. Figure 1 shows the likely source regions for dust
20 sampled during the flights, identified from HYSPLIT simulation and MSG-SEVIRI satellite
21 products. Mineral dust were most likely uplifted from southern Morocco and southern Algeria
22 and were sampled during flights F29, F30, F31 and F32 after 3.5-4.5 days of transport.

23 On 19-20 June the remnants of the aforementioned low are still visible as an upper level
24 trough over the western Mediterranean (Figure S5), triggering meridional transport at higher
25 levels from North Algeria/Tunisia region towards the Sardinia and Sicily Channels. This is
26 confirmed by backward trajectory and satellite product analyses showing that the dust
27 sampled during the flight F33-34 travelled 1 to 5 days from North Algeria/Tunisia before their
28 sampling (not shown). On 28 June during flight F38, an upper level low is found over the
29 Alps and central Europe, inducing a westerly flow from Tunisia where mineral dust were most
30 likely uplifted towards Sicily at 700 hPa (Figure S6), while the surface high pressure over
31 East Atlantic and Iberia is associated to northwesterly winds at lower levels throughout most
32 of the central Mediterranean. Finally, the situation during the last flight F42 (3 July) was
33 characterized by a modest depression over Iberia, while the Azores anticyclone extended
34 towards the Mediterranean. As a consequence, upper level winds were mainly southwesterly

1 over North Africa, veering to westerly or northwesterly over the Sardinia and Sicily Channel,
2 thus contributing to dust transport in the area. We estimate that mineral dust originating from
3 South Morocco and Tunisia was transported for 3.5 days before sampling.

4 The identification of the dust source regions was confirmed by the measurements of the
5 elemental composition. Overall, Si/Al ranged between 2.4-2.7 and Fe/Ca between 0.3-0.7 in
6 the samples collected during ChArMEx/ADRIMED. This is consistent with values previously
7 reported for mineral dust originating from Algeria, Tunisia and Morocco (Scheuvens et al.,
8 2013; Formenti et al., 2014). The identified emission areas also correspond to known source
9 regions such as the Grand Erg Occidental at the border between Algeria and Morocco, the
10 Mekkeranne in Algeria and the Chott El Jerid in Tunisia (Ginoux et al., 2012).

11

12 **3.2. Vertical distribution of mineral dust**

13 Figure 5 shows the vertical profiles of the aerosol scattering coefficient σ_{scat} at $\lambda = 450, 550$
14 and 700 nm, the total particle number concentration in the submicron ($N_{fine}; 5\text{nm} < D_p < 1\ \mu\text{m}$)
15 and the supermicron ($N_{coarse}; D_p > 1\ \mu\text{m}$) size ranges, and the vertical distribution of the
16 scattering Angstrom exponent \hat{A} calculated between 450 and 770 nm. The top height of the
17 boundary layer (Z_b) and the wind shear level (Z_s) are also indicated in Figure 5 by a solid and
18 a dashed line, respectively. All the vertical profiles were characterized by a weak and positive
19 gradient of the potential temperature, characteristic of a stratified atmosphere (Figure S7). The
20 top height of the boundary layer was identified as the height at which the temperature profile
21 showed the highest discontinuity and the water vapor mixing ratio decreased the most rapidly.
22 The shear level was determined from the sudden increase in wind speed and change in wind
23 direction (Figure S7).

24 Mineral dust was observed above the boundary layer in layers extending from 1 km to more
25 than 6 km above sea level (asl) (Figure 5). The presence of mineral dust within the boundary
26 layer was not attested neither by chemical analyses nor with the back-trajectories analyses,
27 which revealed that in the 5 days prior sampling, low-level air masses originated from the
28 European continent or recirculated within Mediterranean basin. The transport of mineral dust
29 in the free troposphere up to 9 km in altitude is a common observation in the Mediterranean
30 region, as previously reported by lidar measurements (Gobbi et al., 2000; Dulac and Chazette,
31 2003; Mona et al., 2006; Di Iorio et al., 2009; Gómez-Amo et al., 2011). Such high altitudes
32 may be linked to the strong vertical convective processes over the dust source regions, which
33 lift dust particles at high atmospheric levels (Flamant et al., 2007, Papayannis et al., 2008;
34 Cuesta et al., 2009).

1The dust vertical structures showed an important variability. Complex and stratified structures
2were observed depending on the position of Z_b and Z_s . During the campaign, the wind shear
3level was equal to or higher than the top of the boundary layer.

4When Z_b and Z_s coincided (F30, F31, F32, F38), the dust vertical structure was characterized
5by a single and rather homogeneous layer. It is noteworthy that apparently similar thermo-
6dynamical situations displayed a different spectral dependence of the scattering coefficient, as
7for example is the case above the boundary layer for flights F32 ($\mathring{A} \sim 0.3$) and F38 ($\mathring{A} \sim 0.9$),
8pointing out differences in the particle type. The values of \mathring{A} observed during the flight F38
9were higher than the values of ~ 0.5 reported for Saharan dust in source region (McConnell et
10al., 2008a; Muller et al., 2011b), but lower than values of $\mathring{A} > 1$ reported for air masses
11dominated by pollution aerosols in the western Mediterranean basin (Di Biagio et al., 2015). It
12is reasonable to suppose that the profile F38 reflects a situation where desert dust was mixed
13with pollution particles. This is confirmed by the five-day backward trajectories (Figure 6a),
14which indicates air parcel coming from Europe and traveling at least three days above the
15Mediterranean Sea within the boundary level before its uplift over Tunisia.

16When Z_s was higher than Z_b (F33, F34, F35), mineral dust was found in two distinct layers
17below and above 3 km asl, respectively. The five-day backward trajectories suggest that these
18dust layers originated from different dust source regions (Figure 1 and Table 1). An example
19is given by the flight F35 (Figure 6b) for which the above-3km dust layer originated from
20central Algeria and was carried by northern flow to Lampedusa in 3.5 days, whereas the
21below-3 km dust layer was transported from the southeastern Morocco-southwestern Algeria
22border region by a westerly flow within 3 days. Similar structure with multilayering of the
23Saharan dust corresponding to air masses from different dust source regions was previously
24observed by lidar measurements in the Mediterranean region (Hamonou et al., 1999;
25Guerrero-Rascado et al. 2008).

26Regardless of the thermo-dynamical structure of the atmosphere, the aerosol vertical profiles
27revealed a clear vertical variability of the contribution of fine mode particles in the dust
28layers. The values of N_{fine} and \mathring{A} were generally below 1000 \# cm^{-3} and 0.5, respectively, in
29dust layers above 3 km asl. In contrast, N_{fine} and \mathring{A} were up to 4000 \# cm^{-3} and 2.2,
30respectively, in the dust layers below 3 km altitude (Figure 5). These observations suggest that
31either the dust plumes carried more fine particles during transport below 3 km altitude or that
32dust particles in the fine mode exhibited a vertical gradient.

33

34

1

2

13.3. Size distribution of the dust plumes

2 Particle number size distributions classified as a function of altitude are shown in Figure 7.
3 Table 3 presents the average characteristics of the parameterized four-modal number size
4 distributions.

5 In the fine mode particle size range, the size distributions showed three modes around 80, 120
6 and 320 nm (Figure 7a). For particles smaller than 300 nm, the shapes of the size distributions
7 in the dust layer and in the boundary layer were quite similar. As particles in this size range
8 mostly reflect anthropogenic influences from near or distant sources (Birmili et al., 2010), this
9 indicates that the pollution plumes from the surface were exported above the boundary layer
10 and mixed with the dust layers. The particle size distributions in the dust layers above 3 km
11 followed a similar pattern as in the dust layers below 3 km but number concentrations 2 times
12 smaller were observed for the modes at 80 and 120 nm, suggesting that the concentration of
13 pollution particles varied with the altitude. For particles between 300 nm and 1 μm , the
14 particle size distributions were reasonably constant for dust layers at various altitudes. Gomes
15 et al. (1990) found dust particles as small as 300 nm diameter in Algeria, which was also
16 confirmed by Kaaden et al. (2008) and Kandler et al. (2009) in Morocco. The decrease of N_{fine}
17 with altitude (i.e. Figure 5) was therefore most likely due to the larger concentration of sub-
18 300 nm pollution particles transported in the dust plumes below 3 km altitude. The fact that an
19 identical median diameter $D_{p,g}$ was used to parameterize the number size distributions in the
20 fine mode for below- and above-3km layers (Table 3) and the prevalence of a sub-300 nm
21 particles in the below-3 km dust layer (Figure 7a) might also reflect that the mixing between
22 the pollution and the dust plumes was mostly external in the fine mode.

23 In the coarse mode, a modal diameter of the number size distribution between 1.3 and 2.0 μm
24 was observed indiscriminate of dust altitude. This indicates that the dust layers transported
25 over the Mediterranean basin were well-mixed vertically in terms of coarse particle
26 population, as previously observed by Weinzierl et al. (2011) for mineral dust after short-
27 range transport over the eastern Atlantic Ocean. Conversely, the number concentration of
28 large dust particles decreased with increasing altitude for freshly uplifted Saharan dust
29 (Weinzierl et al., 2009; Ryder et al., 2013a). There are some evidences suggesting that the
30 good vertical mixing of the dust plumes occurs during the first day following the dust uplifted
31 (Ryder et al., 2013b). Turbulent fluxes within the dust layer might be responsible for the
32 vertical distribution of the dust aerosols becoming more homogeneous in terms of coarse
33 mode particles as the dust ages (Rosenberg et al., 2014). Particles in the coarse mode showed
34 a large flight-to-flight variability with number concentrations varying by more than one order

1 of magnitude. This is quite evident in Figure 7b showing the conversion of number size
2 distributions into volume size distributions. This variation in concentration might reflect the
3 wide range of dust event encountered during the campaign in terms of source regions, time of
4 transport and meteorological conditions.

5 The spread of volume size distributions obtained during ADRIMED overlaps with those
6 measured during other airborne campaigns close to dust source regions (AMMA, FENNEC
7 and SAMUM-1) in the coarse mode size range (Figure 7c). Effective diameters of the coarse
8 mode $D_{eff,c}$ (*i.e.* estimated in the size 1-20 μm as defined in eq. 7) ranged from 3.8 to 14.2 μm
9 during ADRIMED, which is in the range of magnitude of the mean values of 3.8, 8.8 and 7.4
10 μm obtained during AMMA, FENNEC and SAMUM-1, respectively (Formenti et al., 2011b;
11 Ryder et al. 2013a; Weinzierl et al., 2011). Balloonborne observations during ADRIMED also
12 showed the presence of large particles of more than 15 μm in diameter inside dust plumes
13 transported over the Mediterranean basin (Renard et al., 2015). Contrastingly, fewer particles
14 larger than 10 μm were counted after short-range transport over the eastern Atlantic Ocean in
15 the Cape-Verde region during SAMUM-2 with respect to the other campaigns. $D_{eff,c}$ around
16 3.2 μm was found in the dust layers during SAMUM-2 (Weinzierl et al., 2011).

17

18 3.4. Optical properties of the dust plumes

19 Figure 8a-b shows the vertical distribution of the real and imaginary parts of the refractive
20 index \tilde{n} . Within the dust plumes, \tilde{n} ranged from 1.50 to 1.55 for the real part and remained
21 below 0.005 for the imaginary part. Since \tilde{n} is related to the aerosol chemical composition
22 (Liu and Daum, 2008), it is expected to be influenced by the mixing rate of the dust plume
23 with pollution particles. We thus plotted the values of \tilde{n} as a function of \dot{A} . Besides not
24 displaying significant variation with the altitude, the values of \tilde{n} did not show any dependence
25 on \dot{A} . The results obtained during ADRIMED have been compared with data in the literature
26 for Saharan dust in or near-sources in Figure 8. For both the real and imaginary parts, our
27 estimates of \tilde{n} fall within the range of variability (1.51 - 1.57 and 0.0001 - 0.0046 for the real
28 and the imaginary parts, respectively) documented in source regions (Schladitz et al., 2009;
29 Formenti et al., 2011a; Ryder et al., 2013b). This variability was attributed to the variability of
30 the mineralogical composition of dust originating from diverse source regions (Kandler et al.,
31 2009; Petzold et al., 2009). Our data do not show any clear dependence of \tilde{n} on dust source
32 region either (not shown), which is consistent with the limited regional variability of the dust
33 optical properties found 1-2 days after emissions in Africa by Formenti et al. (2014) from
34 aircraft measurements. This is probably a consequence of the mixing of dust plumes from

1various active sources occurring during transport shortly after emission. A number of
2uncertainties in our identification of dust source region is associated with the employed
3methodology. The trajectory error associated with calculation of back trajectories from
4HYSPLIT reaches 15–30 % of the travel distance (Draxler and Rolph, 2013). Another
5potential source of uncertainty is the difficulty to discriminate the satellite aerosol signals
6from the surface reflectance using MSG-SEVIRI observations, especially over bright surfaces
7(Kutuzov et al., 2013). Moreover, even if the origin of the air masses was checked at the
8beginning, the middle and at the end of each SLR, a larger number of sources could
9potentially contribute to a given aircraft sample that covers at least 120 km because of
10aircraft’s movements during SLR sampling.

11The vertical distribution of intensive optical properties relevant to radiative transfer (i.e.
12single scattering albedo ω_0 , asymmetry parameter g and extinction mass efficiency k_{ext}) are
13shown in Figure 8c-e and Table 4. Estimates of ω_0 , g and k_{ext} fall within the range 0.90 - 1.00,
140.6 - 0.8 and 0.2 - 0.7 m² g⁻¹, respectively. Overall, there is no clear dependence on the
15altitude. Only slightly low values of g (from ~0.7 to ~0.8) and k_{ext} (from ~0.2 to ~0.7 m² g⁻¹)
16were observed for some dust layers below 3 km asl. As \tilde{n} was found to be constant with the
17altitude (i.e. Figure 8a-b), these variations in g and k_{ext} were probably due to the variability in
18particles size distributions, which is consistent with the larger fraction of fine particles found
19in the below-3 km dust layers (i.e. Figure 7a). Values of ω_0 , g and k_{ext} remained, however,
20within the range of values reported in source regions by Schladitz et al. (2009), Formenti et
21al., (2011a) and Ryder et al., (2013b). Despite the fact that dust plumes carried pollution
22particles during their long-range transport in the Mediterranean region, the dust optical
23properties appeared to be unaffected by this mixing.

24In the Mediterranean region, previous estimates of ω_0 for dust particles were obtained from
25remote-sensing techniques. Mallet et al. (2013) reported from multi-year ground-based
26AERONET observations a column-averaged ω_0 of 0.92-0.95 between 440-880 nm for various
27sites over the Mediterranean under the influence of dust aerosols. Using a similar approach,
28Di Biagio et al. (2009) reported lower column-averaged ω_0 values during dust transport events
29when boundary-layer air masses are transported from central Europe, probably rich in
30absorbing particles from urban-industrial European areas. Values as low as 0.88 at 530 nm
31were also determined by Sicard et al. (2012) during a case study of a dust plume transported
32over Barcelona and accompanied by a biomass-burning outbreak. Recently, Valenzuela et al.
33(2014) presented eight months of dust optical properties over the Alborán Island from Sun
34photometer measurements for dust plumes originating from northwestern Africa and passing

1 over several urban-industrial areas along the coast of Morocco and from northeastern Africa
2 and traveling over the Mediterranean Sea. No significant changes in column-averaged ω_0 were
3 reported for the different air masses, which indicates that the influence of anthropogenic fine
4 particles originating from the urban-industrial areas in the north of Africa during desert dust
5 outbreaks was negligible. Overall, these contrasting results highlight the major role of the
6 transport conditions (height, air mass encountered) of the dust plumes in governing the
7 mixing processes of mineral dust with other aerosol species.

8

9 4. Discussion

10 4.1. On the role of transport conditions in the mixing of pollution particles 11 with mineral dust

12 In this section, we investigate the transport conditions of the dust layers expected to influence
13 the mixing of mineral dust with pollution particles. As previously mentioned, the highest
14 concentrations of pollution particles were detected in the below-3 km dust layers. We further
15 investigate this result by examining the variations of $D_{eff,f}$ and $D_{eff,c}$ with the altitude of the dust
16 plumes. We assume that changes in $D_{eff,f}$ reflected different fractions of externally mixed
17 pollution particles smaller than 300 nm in the dust plumes, as discussed in section 3.3. In
18 Figure 9a, a sharp transition in the proportion of fine particles can be seen in $D_{eff,f}$ at 3 km asl.
19 with greater proportion of pollution particles found in the lower 3 km of the atmosphere. The
20 observation of pollution particles at altitudes up to 3 km during ADRIMED is compatible with
21 the average height of pollution layers observed in the western Mediterranean basin (Meloni et
22 al., 2003; Mallet et al., 2005; Junkermann et al., 2009; Di Biagio et al., 2015). Hence, the
23 vertical extent of pollution particles might explain the fact that the below-3km dust plumes
24 were more affected by fine particles than the above-3km dust layer. The coarse mode of the
25 dust plume is also expected to be impacted by the presence of pollution particles in case of an
26 internal mixing between pollution particles and mineral dust, which should somewhat
27 increase the mean particle size. During ADRIMED, $D_{eff,c}$ of the dust plume did not show any
28 systematic dependence on altitude (Figure 9b). This finding must however be interpreted with
29 some caution since $D_{eff,c}$ was affected by the large uncertainties in FSSP-300 and GRIMM
30 sizing (i.e. section 2.2.1.) that might hide the detection of the effect on particle size of an
31 aggregation of small pollution articles onto mineral dust particles.

32 The mixing extent of pollution particles in dust layers is also expected to depend on the
33 transport time of the plumes. Figure 10 shows $D_{eff,f}$ against the estimated age of the dust air
34 mass and divided according to the height of transport of the dust plumes. From these

1 measurements, we do not find any significant trend in the dust mixing rate with transport time
2 in both below- and above-3km layers. This result is not surprising for the above-3km dust
3 layers since we found that the interaction of dust plumes with pollution particles was limited
4 when they were transported above 3 km asl. For dust plumes below 3 km asl., their transport
5 time was at least 3 days before sampling during ADRIMED. Afterwards the time spent by
6 dust over pollution regions appeared to have no more effect on the mixing extent of pollution
7 particles. The constant D_{eff} values observed within the below-3km dust plumes and the
8 boundary layer (Figure 9a) suggests also that the vertical transport and mixing of pollution
9 particles within dust plumes were already completed at the time of sampling. Note that the
10 below-3km dust layers reached the Mediterranean coasts affected by urban/industrial
11 emissions after having undergone around 2 days of transport. Hence, the pollution mixing rate
12 appears to be a relatively rapid process more likely driven by the height of transport of the
13 dust layers.

14

15 **154.2. Contribution of pollution particles to the absorption properties of the** 16 **dust plumes**

17 We evaluated the effect of the contribution of pollution particles to the absorption properties
18 of the dust layers by calculating ω_0 from the mass concentration of the main anthropogenic
19 compounds. Table 5 shows the mass concentration of major elements, ionic species and rBC
20 measured in the dust plumes. The dust mass concentration estimated from the measured Al
21 using the mean Al mass fraction in the crustal composition of 7.09% (Guieu et al., 2002) is
22 also shown. In all samples, silicates were the most abundant type of dust particles, as expected
23 from previous chemical analysis of dust in North Africa (Scheuvens et al., 2013; Formenti et
24 al., 2014). The presence of pollution particles within the dust plumes is confirmed by the
25 detection of SO_4^{2-} and rBC as well as typical anthropogenic trace elements such as V, Pb and
26 Zn.

27 SO_4^{2-} reached concentrations typical of the Mediterranean region in summertime (Ripoll et al.,
28 2015) with the largest concentration of $2.5 \mu\text{g m}^{-3}$ found over Corsica during the flight F34.
29 The positive correlation between the concentration of SO_4^{2-} and N_{fine} indicates the presence of
30 externally mixed sulfate-containing particles in the fine mode particles, such as ammonium
31 sulfate particles. $\text{SO}_4^{2-}/\text{NH}_4^+$ ratios being higher than unity, the presence of SO_4^{2-} in the dust
32 layers can also either be due to nucleation of sulfuric acid in polluted plumes, or to sulphate
33 formation at the surface of preexistent particles by uptake of gaseous sulfur dioxide or by

1coagulation of sulphate particles (Ullerstam et al., 2002; Korhonen et al., 2003; Sullivan et al., 22009).

3Concentrations of rBC ranged from 0.04 to 0.13 $\mu\text{g m}^{-3}$. Although these values are much
4lower than concentrations measured in areas of high industrial or traffic density (Liu et al.,
52014; Mantas et al., 2014), they are in agreement with concentrations found in continental and
6background area of the western Mediterranean (Ripoll et al., 2015). Except in the case of large
7forest fires, rBC concentrations are generally low on average in summertime due to the
8absence of the major sources of emission, such as domestic wood burning (Tsyro et al., 2007).

9Calculations of ω_0 from the aerosol chemical composition were performed assuming that dust
10was externally mixed with rBC and sulfate. Indeed, prevalence of an external mixing between
11dust particles and rBC has been observed from long-term measurements in the western
12Mediterranean basin (Ripoll et al., 2015). Moreover, coating of sulfate on mineral dust has
13been shown to have no significant effect on dust optical properties (Bauer et al., 2007).
14Calculations of ω_0 at 530 nm were performed as follows:

$$\omega_0 = \frac{\sum_j (k_{ext,j} - k_{abs,j}) \cdot C_{m,j}}{\sum_j k_{ext,j} \cdot C_{m,j}} \quad (9)$$

15We used mean mass absorption and extinction efficiencies (i.e. the total light absorption or
16extinction per unit mass of aerosol, referred as k_{abs} and k_{ext}) of 0.02 $\text{m}^2 \text{g}^{-1}$ and 0.64 $\text{m}^2 \text{g}^{-1}$ for
17dust (Hess et al., 1998), 7.5 $\text{m}^2 \text{g}^{-1}$ and 9.4 $\text{m}^2 \text{g}^{-1}$ for rBC (Bond and Bergstrom, 2006) and 0
18 $\text{m}^2 \text{g}^{-1}$ and 5.0 $\text{m}^2 \text{g}^{-1}$ for sulfate (Charlson et al., 1992). As shown in Table 5, ω_0 obtained from
19this calculation ranged from 0.93-0.97, which falls within the range of values obtained from
20measurements (0.92-0.99). For comparison, we estimate that ω_0 for pure mineral dust was
210.97. This simple approach confirms the small influence of pollution particles on the optical
22properties of the dust plumes over the western Mediterranean region.

23The ChArMEx/ADRI MED field campaign was characterized by moderate AOD with
24averaged values ranging between 0.1 – 0.6 at 440 nm as observed by AERONET/PHOTONS
25sun-photometers (see Figure 19 of Mallet et al., 2015). Outside of dust events, the AOD
26displayed values from 0.1 to 0.2 (440 nm), while it reached values up to 0.8 under dusty
27conditions. Although higher AOD values have already been observed in the Mediterranean
28region during intense pollution or biomass burning events (Pace et al., 2005; Alados-
29Arbodelas et al., 2011; Péré et al., 2011), values obtained during ADRI MED are typical of
30those observed in summertime (Nabat et al., 2015). This observation is also supported by the
31mass concentration of the main anthropogenic compounds that reached typical values for the

1 region, as discussed previously. Our result on the moderate absorption properties of the dust
2 plumes is thus likely relevant to dust events in the western Mediterranean in the absence of
3 intense pollution or biomass burning emissions and can be used for constraining modeling
4 studies and satellite retrievals that make assumption on dust optical properties.

5 We compared our measurements on dust absorption properties with values published in the
6 OPAC aerosol database that is widely used by modelling and remote sensing communities.
7 The result of this comparison indicates an overestimation of dust absorption properties in the
8 OPAC database. The n_i value achieved in the OPAC database ($n_i=0.006-0.008$ at 550-500 nm,
9 respectively) are high compared to values observed for Saharan mineral dust in source region
10 and over the Mediterranean during ADRIMED (n_i between 0.000-0.005 at 530nm). This
11 finding is in line with previous studies showing disagreements in dust absorption between
12 satellite retrievals and modelling studies that has been solved by decreasing the imaginary part
13 of the dust refractive index (Kaufman et al, 2001; Moulin et al, 2001; Balkanski et al., 2007;
14 Mian Chin et al., 2009).

15

16 4.3. Retention of coarse mode particles in the dust plumes

17 Figure 11 shows $D_{eff,c}$ against the estimated age of the dust air mass. Observations from
18 aircraft during previous campaigns are shown for comparison. The $D_{eff,c}$ values did not change
19 with time, suggesting that the dust layers transported over the Mediterranean region tend to
20 conserve their coarse mode with time. During ADRIMED, $D_{eff,c}$ values obtained in dust layers
21 having spent less than 1.5 days in the atmosphere are consistent with those obtained near dust
22 source regions (Formenti et al, 2011b; Weinzierl et al., 2011). Conversely, dust layers having
23 spent more than 1.5 days in the atmosphere present higher $D_{eff,c}$ than previously observed over
24 the Atlantic ocean (Maring et al., 2003; Weinzierl et al., 2011). The loss of large dust particles
25 after transport as observed over the Atlantic Ocean is most likely associated to the removal
26 processes occurring as the dust travels downwind (Mahowald et al., 2014). As smaller
27 particles fall downward much slower than larger particles, coarse particles are expected to be
28 more prevalent close to the sources regions. To date only few studies have focused on
29 understanding the evolution of dust size distribution, especially during transport over the
30 Atlantic Ocean (Maring et al., 2003; Reid et al., 2003; Kalashnikova and Kahn, 2008). These
31 measurements pointed out large differences between the observed and modeled evolution of
32 dust size, with a lifetime of coarse particles longer than expected from deposition theories.
33 This suggests that other processes counterbalanced the loss of large particles by dry
34 deposition along transport. These processes seem to be particularly important in the

1Mediterranean region, since the proportional volume of coarse particles in the size distribution
2did not vary substantially even after 5 days of transport.

3The persistence of coarse particles over the Mediterranean basin during transport could be
4explained by the presence of temperature inversions in the middle troposphere keeping the
5dust layers confined due to the stable stratification. This was revealed by most of the aircraft
6temperature profiles (Figure S7). Furthermore, the WRF model simulations of the vertical
7velocity and vertical cross-section confirms previous indications (Dulac et al., 1992) of the
8existence of updraft/downdraft due to the thermal turbulence within the dust layers circulating
9over the Mediterranean basin in summertime, due to elevated temperatures within the dust
10layers and large insolation. An example for flight F33 in the Corsica region is shown in Figure
1112, where the vertical velocity showed updrafts and downdrafts up to 0.5 Pa s^{-1} , corresponding
12to about 5 cm s^{-1} . This value is at least one order of magnitude greater than the gravitational
13settling velocity (0.25 cm s^{-1}) expected for particles of $8 \text{ }\mu\text{m}$ in diameter, value indicated by
14Maring et al. (2003) as the threshold above which sensible changes in dust size distribution
15during atmospheric transport across the Atlantic could be observed. The occurrence of
16turbulent updraft and downdraft motion could therefore result in an enhancement of the
17particle lifetime in the atmosphere over the Mediterranean basin.

18

195. Conclusions

20We presented the first *in situ* aircraft measurements of the size distribution and optical
21properties of Saharan dust transported over the western Mediterranean basin obtained within
22the framework of the ChArMEx/ADRIMED airborne campaign in June-July 2013. Dust
23particles originating from Algeria, Tunisia and Morocco were sampled in the western
24Mediterranean basin after 1 to 5 days of transport from the source regions.

25Measurements of aerosol vertical profiles revealed that dust particles were transported inside
26well-defined layers above the boundary layer ($>1 \text{ km asl.}$), itself dominated by pollution and
27marine particles. The dust vertical structure was extremely variable and characterized either
28by a single layer or a more complex and stratified structure. Backward trajectories indicated
29that the multilayering of the Saharan dust corresponded to air masses originating from
30different dust source regions. Abundance of sub-300 nm particles in the Saharan dust layers
31suggested a strong mixing of dust with pollution particles. The height of transport of the dust
32layers appeared to be the main factor affecting the mixing extent of pollution particles with
33mineral dust. Measurements showed higher concentration of pollution particles in dust layers
34below 3 km asl. than at higher altitude, resulting in \bar{A} up to 2.2 below 3 km asl. This coincides

1with the typical height of pollution layers (~3 km asl.) observed in the western Mediterranean
2basin.

3The optical properties of the dust layers were not significantly affected by this mixing with
4respect to values reported for native dust. Mineral dust aerosols were found to be moderately
5absorbing with values of ω_0 between 0.90 and 1.00 at 530 nm. Concurrent optical calculations
6from the aerosol chemical composition revealed that the contribution of pollution particles to
7absorption properties of the dust plumes was negligible. This was most likely due to the low
8contribution of rBC (~2% in mass) in regards to the fraction of dust (~84%) and sulfate
9(~14%) in the dust plumes. The concentrations of anthropogenic particles being typical of
10those observed in the Mediterranean region in summertime, these results demonstrate that
11outside outside a severe episode of pollution or biomass burning, mineral dust dominate the
12optical properties of the dust plumes in the Mediterranean even in the presence of pollution
13particles.

14An important question for the dust direct, semi-direct and indirect radiative effects is how
15long the coarse mode of dust particles is conserved during transport. We showed that the
16coarse mode was conserved even after 5 days of transport in the Mediterranean, which
17contrasts with the gravitational depletion of large dust particles observed during the transport
18of dust over the Atlantic Ocean. The global importance of this result is, however, still linked
19to whether these observations are ubiquitous or occur only for specific dust transport events.
20Dust events differing in terms of source region, time and height for transport were reported in
21this study. For all these case studies, the coarse mode of dust particles was conserved during
22transport, which might reflect the representativeness of the situation mostly occurring in
23summertime in the western Mediterranean basin.

24Most climate models currently simulate the dry deposition as a positive relationship of the
25particles size, leading in an underestimation of the fraction of coarse particles being
26transported long distances (Mahowald et al., 2014). Given the scarcity of field studies
27investigating the evolution of the dust size distribution during transport, our results point out
28key processes controlling the retention of large dust aerosols particles. In particular, WRF
29model simulations highlighted a strong turbulence within the dust layer with vertical velocity
30at least one order of magnitude greater than the particle gravitational settling velocity.
31Particles could therefore remain trapped in the atmosphere by this strong turbulence. Further
32studies involving a deep analysis of aircraft measurements of turbulence parameters both in
33the Mediterranean and in other geographical areas such as the Atlantic region are required in
34order to quantitatively characterize this process and improve the representativeness of the

1 temporal evolution of dust size distribution in climate models useful for radiative impact or
2 marine biogeochemical applications.

3 The dataset obtained during the ChArMEx/ADRIMED airborne campaign can also be used
4 for constraining satellite retrievals that make assumptions on dust properties in order to derive
5 water vapor profiles, surface temperatures and greenhouse gases concentrations. The results
6 presented here suggest that the aerosol particle size and optical properties of the dust plumes
7 could be assimilated to those of native dust in satellite retrievals in the western Mediterranean.
8 A straightforward comparison of our results with values published in the OPAC aerosol
9 database, which is widely used by the remote sensing communities, suggests that the OPAC
10 database overestimate dust absorption. Moreover, this important dataset provides
11 opportunities for evaluating satellite aerosol products (size, absorption properties, vertical
12 profiles) over the Mediterranean through comparison with our in-situ airborne measurements.
13 In terms of significance for direct and semi-direct radiative effects, the presence of moderately
14 absorbing particles within the dust layers can induce important modifications in the
15 tropospheric heating and surface cooling by perturbing the incoming and outgoing radiations.
16 Evidence for retention of coarse mode particles in the dust layers indicates also that mineral
17 dust may still be a significant source of cloud condensation nuclei and ice nuclei despite
18 having undergone long-range transport. Hence, mineral dust may have potentially important
19 implications for the regional climate and the rainfall patterns in the western Mediterranean
20 that should be quantitatively addressed in future modelling studies.

21

22 **Acknowledgements**

23 This research work has been supported by the French National Research Agency (ANR)
24 through the ADRIMED program (contract ANR-11-BS56-0006). This work is part of the
25 ChArMEx project supported by CNRS-INSU, ADEME, Météo-France and CEA in the
26 framework of the multidisciplinary program MISTRALS (Mediterranean Integrated Studies
27 at Regional And Local Scales; <http://mistrals-home.org/>). The aircraft deployment was also
28 supported by CNES. We thank the instrument scientists, pilots and ground crew of SAFIRE
29 for facilitating the instrument integration and conducting flight operations. We acknowledge
30 Pierre Nabat and the ENM students, especially Damien Serça, Jonathan Guth and Valentin
31 Seigner for their meteorological forecasts during the campaign. We thank the NOAA Air
32 Resources Laboratory (ARL) for the provision of the HYSPLIT transport and dispersion
33 model used in this study. We gratefully acknowledge the two anonymous reviewers whose
34 suggestions helped us improving and clarifying this manuscript.

Table 1: Detailed information about the flights (number (ID), date, take-off time (TO), landing time (L) and route), the vertical profiles (latitude (Lat), longitude (Lon) and start time) and the dust layers sampled (height in meter, origin, age in day) during the ChArMEx/ADRIMED airborne campaign. Times are expressed in Coordinated Universal Time (UTC).

6

Flight information					Vertical profile			Dust layer		
ID	Date	TO	L	Flight route	Lat	Lon	Start time	Height	Origin	Age
F29	16 June 2013	08:18	10:20	Cagliari - Minorca	40N	5E	09:50	2200-4500	southwestern Algeria	4.5
F30	16 June 2013	11:58	14:40	Minorca - Granada	37N	4W	14:20	2400-4800	southwestern Algeria	4
F31	17 June 2013	07:15	09:54	Granada - Minorca	37N	4W	07:15	2800-5400	southern Algeria	3.5
F32	17 June 2013	11:45	13:43	Minorca - Cagliari	40N	5E	11:45	1000-4600	southwestern Algeria	4.5
F33	19 June 2013	11:35	15:00	Cagliari - East Corsica	43N	9E	12:50	3000-4000	northeastern Algeria	2
								1500-3000	northeastern Algeria	3
F34	20 June 2013	11:00	14:15	Cagliari - West Corsica	43N	7E	12:20	>2800	Tunisia	1
								1600-2800	Tunisia	5
F35	22 June 2013	08:47	11:26	Cagliari - Lampedusa	36N	13E	10:25	>3500	southern Algeria	2
								1500-3500	southern Morocco	4
F38	28 June 2013	10:59	13:29	Cagliari - Lampedusa	36N	13E	12:30	1200-4500	Tunisia	3
F42	03 July 2013	08:29	11:55	Cagliari - Lampedusa	36N	13E	09:50	>3000	Tunisia	3.5
								<3000	southern Morocco	3.5

7

Table 2: Instruments detailed in this article operating onboard the ATR-42 aircraft during the 2ChArME_x/ADRI_{MED} campaign. The cut-off diameter value, expressed as optical equivalent, is 12 μm for the AVIRAD inlet and 5 μm for the CAI.

4

Parameter measured	Instrument	Abbreviation	Location in the aircraft	Wavelength (nm)	Nominal size range (μm)	Temporal resolution
Size distribution	Forward Scattering Spectrometer Probe, Model 300, Particle Measuring Systems	FSSP-300	wing-mounted	632.8	0.28 - 20	1 s
	Ultra High Sensitivity Aerosol Spectrometer, Droplet Measurement Technologies	UHSAS	wing-mounted	1054	0.04 - 1	1 s
	Sky-Optical Particle Counter, Model 1.129, Grimm Technik	GRIMM	AVIRAD inlet	655	0.25 - 32	6 s
	Scanning mobility particle sizer, custom-built (Villani et al., 2007)	SMPS	community aerosol inlet	n/a	0.03 - 0.4	2 min
Integrated number concentration	Condensation Particle Counters, Model 3075, TSI	CPC	AVIRAD inlet	n/a	> 0.005	1 s
Chemical composition	Filter sampling	n/a	AVIRAD inlet	n/a	n/a	20-40 min
	Single particle soot photometer, Droplet Measurement Technologies	SP2	community aerosol inlet	1064	0.08 - 0.5	1 s
Scattering coefficient	3λ Integrated Nephelometer, Model 3563, TSI	Nephelometer	AVIRAD inlet	450, 550, 700	n/a	1 s
Extinction coefficient	Cavity Attenuated Phase Shift, Aerodyne Research Inc.	CAPS	community aerosol inlet	530	n/a	1 s

n/a: not applicable

6

1Table 3: Parameters (geometric median diameter $D_{p,g,i}$ in μm , geometric standard deviation σ_i ,
2and integrated number concentration $N_{tot,i}$ in $\# \text{cm}^{-3}$) of the four log-normal modes i used to
3parameterize the number size distributions obtained at the different altitudes. The mean,
4minimum and maximum of all parameters are listed.

5

		$D_{p,g,1}$	σ_1	$N_{tot,1}$	$D_{p,g,2}$	σ_2	$N_{tot,2}$	$D_{p,g,3}$	σ_3	$N_{tot,3}$	$D_{p,g,4}$	σ_4	$N_{tot,4}$
Above-3 km dust layer	mean	0.08	1.25	170	0.12	1.60	300	0.32	1.70	15	1.3	2.2	3.0
	min	0.09	1.20	80.0	0.13	1.30	80.0	0.18	1.65	40	2.5	1.8	0.1
	max	0.08	1.25	320	0.12	1.56	600	0.32	1.70	45	1.3	2.2	12
Below-3 km dust layer	mean	0.08	1.25	300	0.12	1.60	700	0.32	1.70	15	2.0	2.4	1.0
	min	0.08	1.25	250	0.11	1.50	400	0.20	1.70	35	1.7	2.1	0.7
	max	0.08	1.25	600	0.13	1.50	1100	0.18	1.90	80	1.7	2.0	2.5
Boundary layer	mean	0.08	1.25	450	0.12	1.60	650	0.32	1.70	5.0	1.3	2.1	1.0
	min	0.08	1.25	150	0.12	1.60	200	0.30	1.70	1.8	1.0	2.1	0.1
	max	0.08	1.25	600	0.12	1.60	1400	0.32	1.70	15	1.3	2.1	3.0

6

7

8

1Table 4: Aerosol optical parameters (real part of the complex refractive index n_r , imaginary
2part of the complex refractive index n_i , single scattering albedo ω_0 , asymmetry parameter g
3and mass extinction efficiency k_{ext}) all at $\lambda=530$ nm as a function of the altitude. The mean,
4minimum and maximum of all parameters are listed.

5

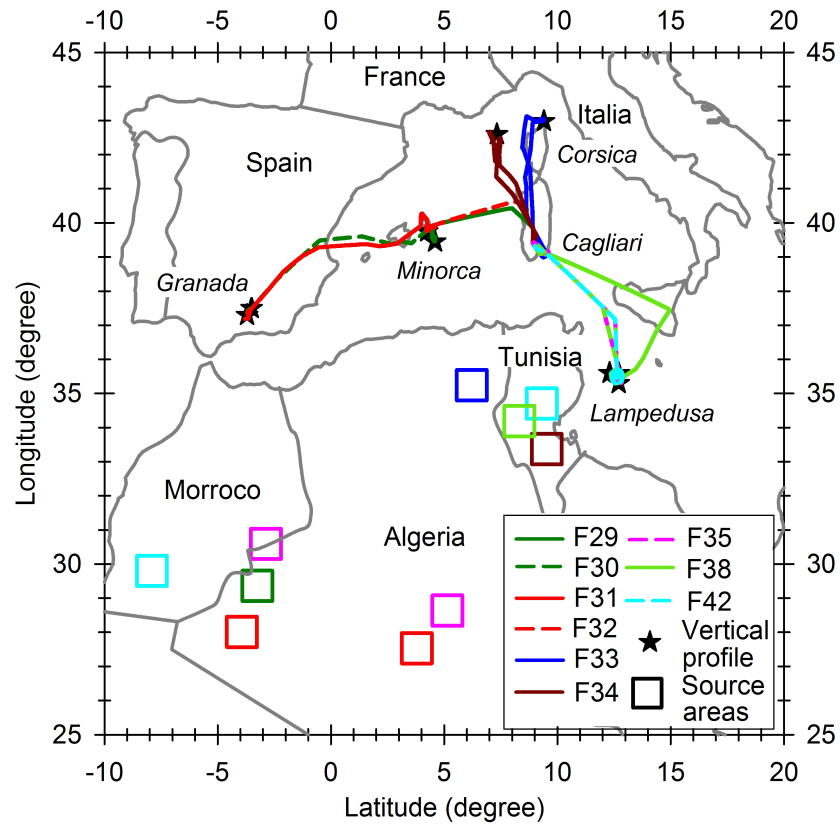
		n_r	n_i	ω_0	g	k_{ext}
Above-3 km dust layer	mean	1.53	0.003	0.95	0.8	0.4
	min	1.50	0.000	0.90	0.7	0.3
	max	1.55	0.005	1.00	0.8	0.5
Below-3 km dust layer	mean	1.52	0.003	0.94	0.7	0.5
	min	1.50	0.000	0.90	0.6	0.4
	max	1.55	0.005	1.00	0.7	0.7

Table 5: Concentrations of major crustal (Si, Al, Fe and Ca, in ng m^{-3}) and metallic tracers (V, Pb and Zn, in ng m^{-3}), ionic species (SO_4^{2-} , NO_3^- , NH_4^+ , in ng m^{-3}), black carbon (in ng m^{-3}), mineral dust (in $\mu\text{g m}^{-3}$) and integrated fine mode of particles (in $\# \text{cm}^{-3}$) during the ChArMEx/ADRIMED airborne campaign. Dash indicates that the specie concentration was slower than the detection limit. The dust mass concentration was estimated from the measured Al using the mean Al mass fraction in the crustal composition of 7.09 % (Guieu et al., 2002). A comparison of the aerosol single scattering albedos ω_0 measured by the nephelometer and CAPS with those estimated from chemical measurements is also shown. The absolute error associated with ω_0 obtained from measurements is 0.04.

10

Flight number	F29	F30	F31	F32	F33	F34	F35	F38	F42
Si	3607	4955	4159	592	2426	9814	6430	2040	5366
Al	1404	2028	1719	225	975	3770	2519	746	2146
Fe	687	1085	845	146	536	1869	1239	416	1032
Ca	1099	1596	1547	-	1322	6404	2112	1374	1592
V	9	6	5	17	16	22	19	13	-
Pb	82	458	28	216	417	-	762	-	-
Zn	20	34	25	4	-	-	71	-	-
SO_4^{2-}	-	1740	-	2016	1574	2505	966	1764	2011
NO_3^-	-	-	-	206	-	285	309	-	467
NH_4^+	-	809	276	640	563	613	-	557	-
rBC	62	97	64	130	57	97	37	97	78
Dust	15.1	21.7	18.4	2.4	10.5	40.5	27.0	8.0	23.0
N_{fine}	316	416	457	881	515	988	229	485	714
ω_0 (measured)	0.97	1.00	0.99	0.92	0.98	0.94	0.97	0.94	0.99
ω_0 (chemistry)	0.93	0.96	0.95	0.94	0.96	0.96	0.97	0.94	0.96

1Figure 1. Operating region of the ATR-42 aircraft during the ADRIMED flights that
 2performed mineral dust measurements. Colors of the lines and squares correspond to the
 3different flights. The positions of the middle of the profiles are shown in black stars. Squares
 4indicate likely sources regions of the dust sampled during the flights (see section 3.1 for
 5identification methodology). The aircraft was based at Cagliari in Sardinia.



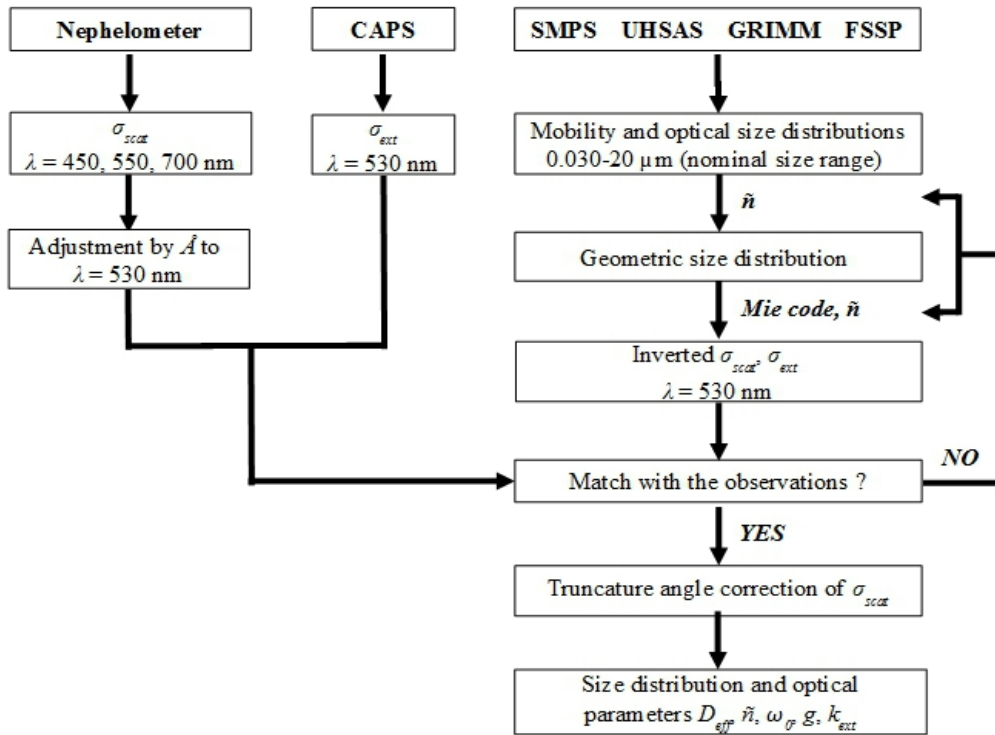
6

1
2

1

2Figure 2: Data inversion procedure to retrieve the dust size distribution and optical
3parameters.

4

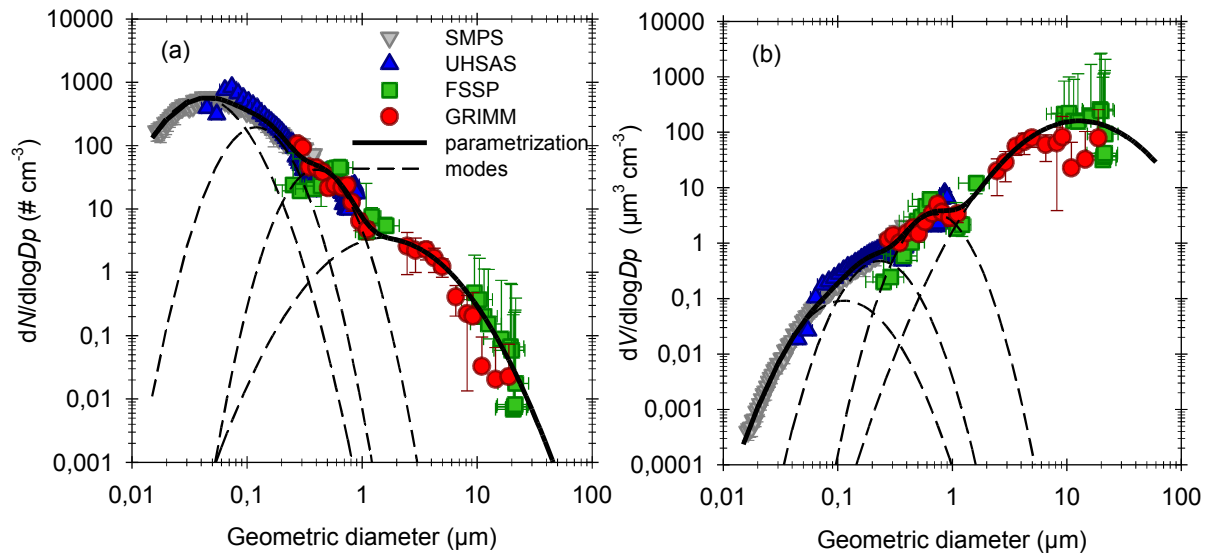


6

1

2

1Figure 3. Number (a) and volume (b) size distributions obtained by the SMPS (gray), UHSAS
 2(blue), FSSP (green) and GRIMM (red) during the flight F35 including refractive index
 3corrections for $\tilde{n} = 1.53 - 0.004i$. Vertical errors bars indicate one standard deviation of the data
 4during the SLR. Horizontal errors bars display the bin sizing uncertainties of the instruments.
 5The dark line represents the parameterized fit with a sum of four log-normal modes (shown in
 6dashed lines).

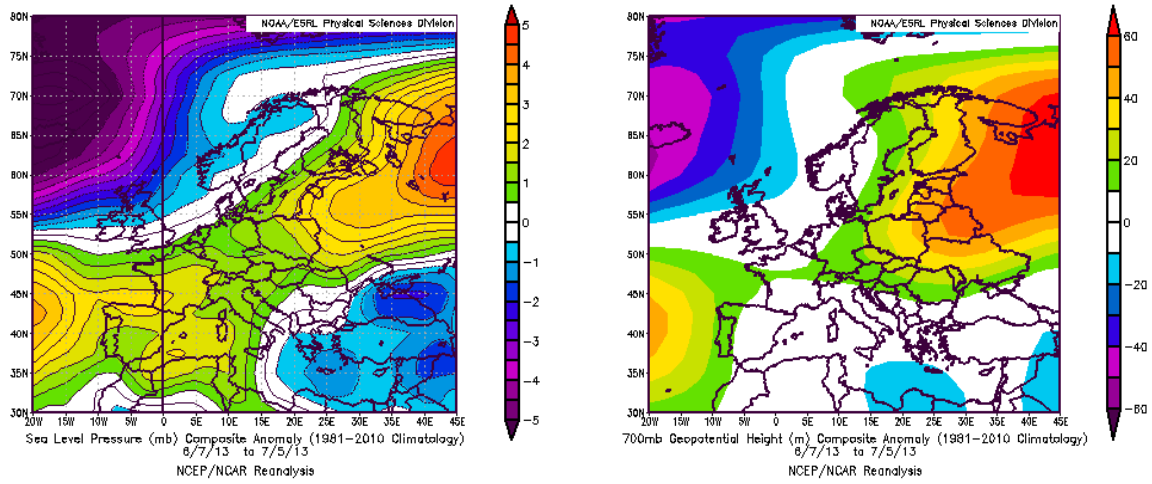


8
 9

1
 2

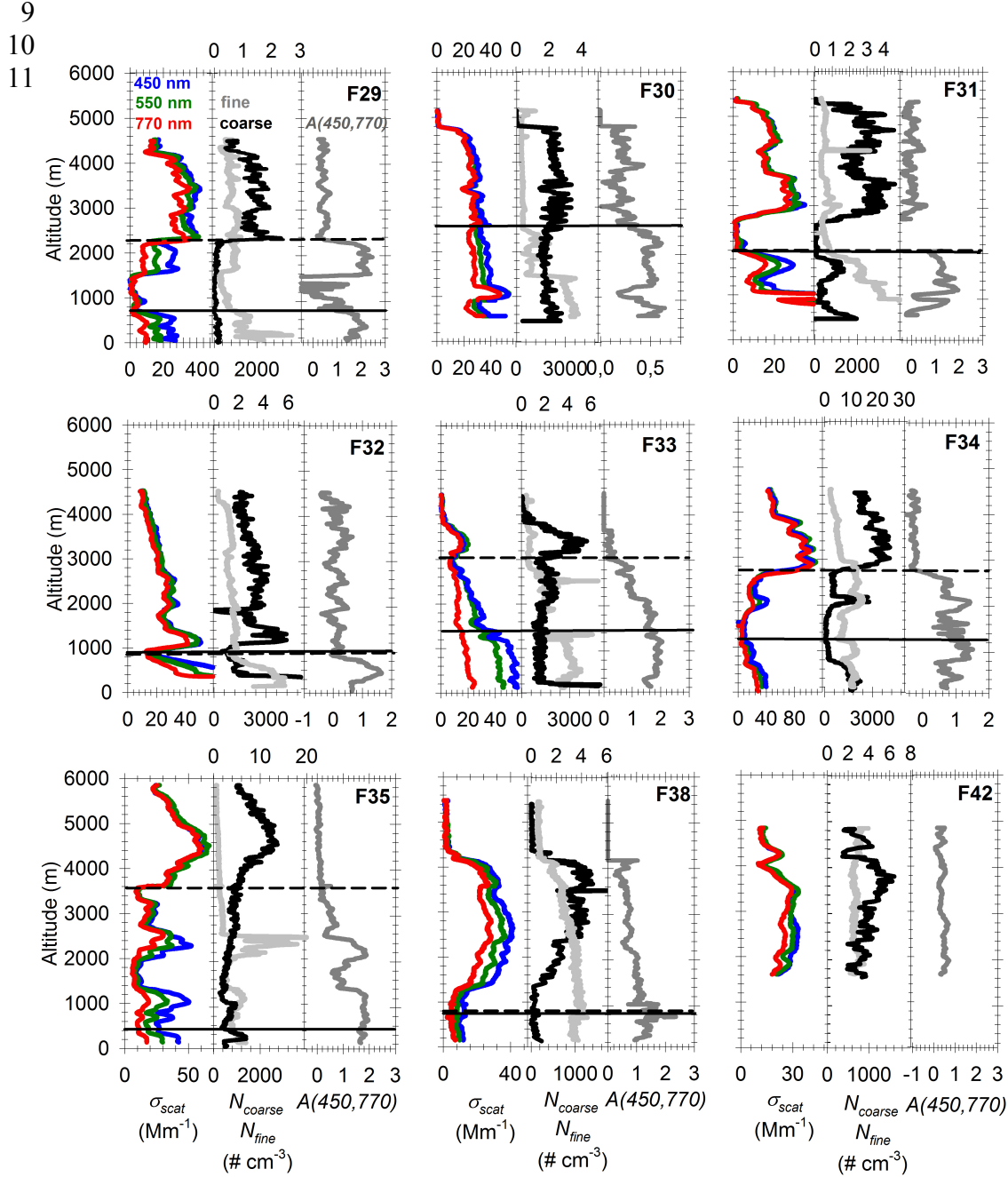
1Fig. 4. Sea level pressure in hPa (left) and 700 hPa geopotential height in m (right) composite
 2mean anomalies over the period from 7 June to 5 July, 2013, with respect to the 1981-2010
 3climatology obtained from the NCEP/NCAR Reanalysis (images provided by the
 4NOAA/ESRL Physical Sciences Division, Boulder Colorado, from their web site at
 5<http://www.esrl.noaa.gov/psd/>).

6



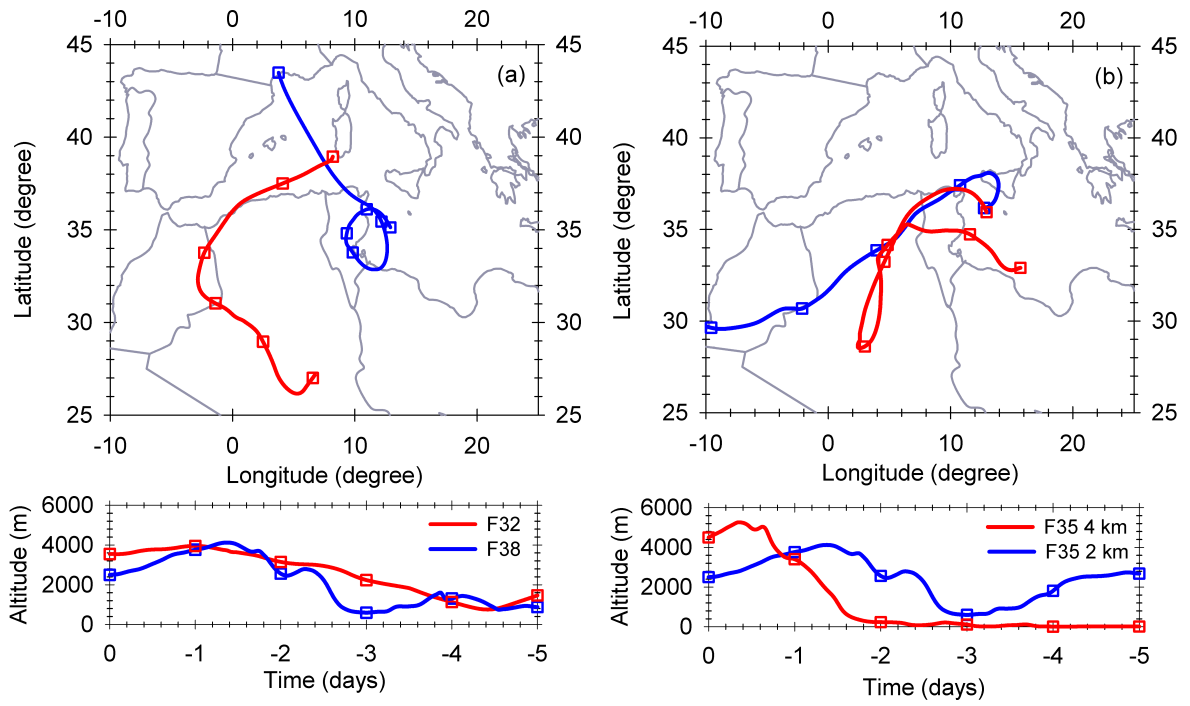
7

1 Figure 5. Vertical profiles of the aerosol scattering coefficient σ_{scat} at $\lambda=450, 550$ and 770 nm
 2 (blue, green and red), the particle number concentration in the submicron N_{fine} (light grey) and
 3 the supermicron N_{coarse} (dark) size ranges and the scattering Ångström exponent \hat{A} calculated
 4 between 450 and 770 nm (dark grey). N_{coarse} is plotted using the upper horizontal axis. The top
 5 of the boundary layer Z_b and the wind shear level Z_s are indicated by a horizontal line and in
 6 dashed line, respectively. The height of Z_b was situated below the minimum flight level in F30
 7 and F42. The height of Z_s was situated below the minimum flight level in F42. Data were
 8 corrected for Standard Temperature and Pressure (STP) using $T=20^\circ\text{C}$ and $P=1013.25$ hPa.



1Figure 6. Five-day backward trajectories calculated for (a) flights F32 and F38 and (b) flight
2F35 arriving at 2 km asl and 4 km asl altitudes in blue and red, respectively.

3



4

5

1

2

Figure 7. Particle size distributions obtained in the dust layers during ADRIMED for (a) number distribution, (b) volume distribution and (c) volume distribution normalized by the total volume concentration. In Figures (a) and (b), size distributions are classified as a function of the altitude of the layer: dust layer above 3 km asl (red), dust layer between 1.5-3 km asl (blue) and the boundary layer below 1 km (green). The shading represents the range throughout the campaign. In Figure (c), the mean (dark line), minimum and maximum normalized size distributions (grey shading) observed above 1.5 km during the ChArMEx/ADRIMED campaign are compared with those observed in the source region during the airborne campaigns AMMA (red line, Formenti et al., 2011a), FENNEC (blue line, Ryder et al., 2013b) and SAMUM-1 (dark green line, Weinzierl et al., 2009), as well as with measurements at Cape-Verde region during SAMUM-2 campaign (light green line, Weinzierl et al., 2011). The AMMA curve (Formenti et al., 2011) is curtailed to 0.3 μm since there was no measurement below this size during the campaign.

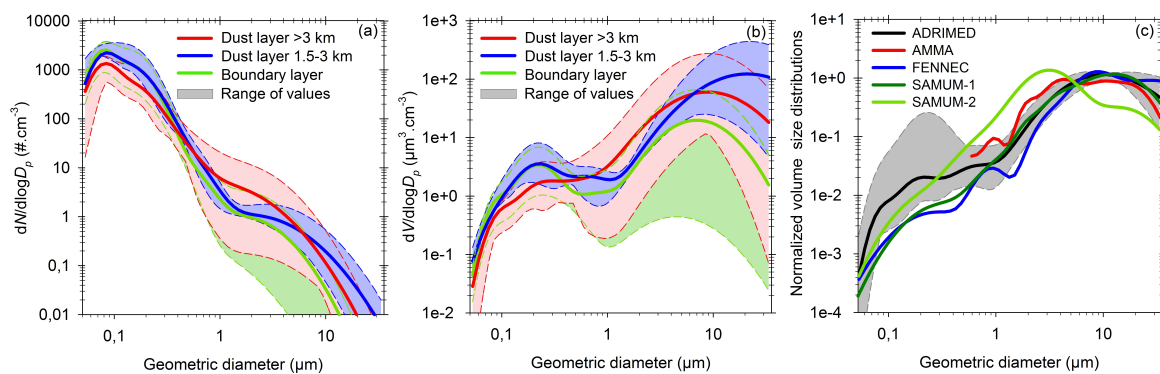
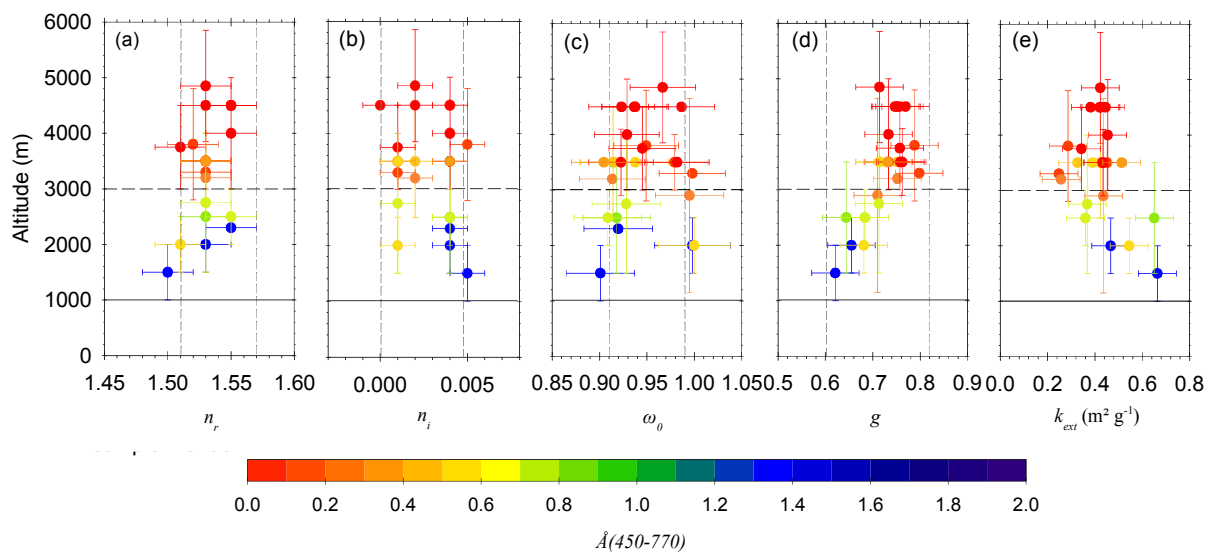


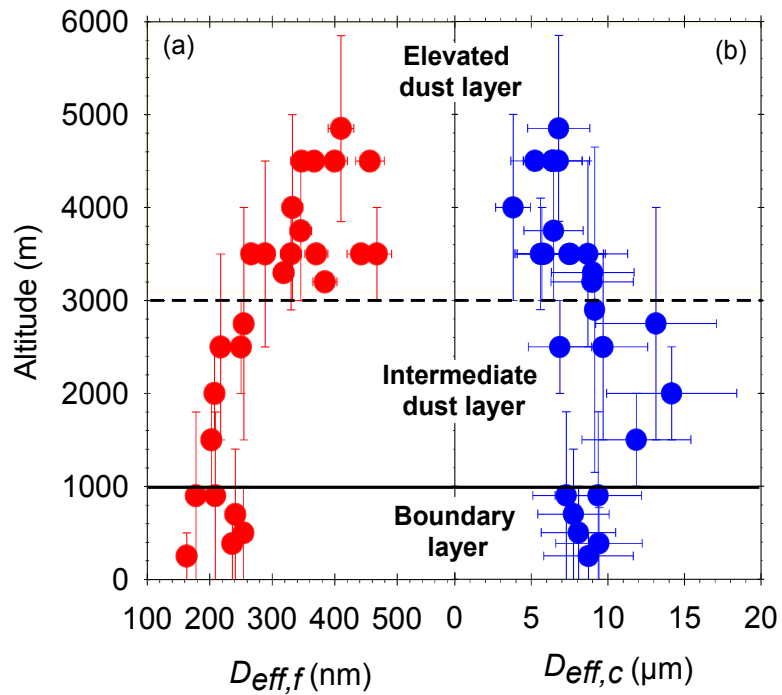
Figure 8. Scatter plots showing (a) the real part of the complex refractive index n_r , (b) the imaginary part of the complex refractive index n_i , (c) the single scattering albedo ω_0 , (d) the asymmetry parameter g and (e) the mass extinction efficiency of aerosols k_{ext} all at $\lambda=530$ nm as a function of the altitude from all SLR and vertical profiles within the dust layers measured during the campaign. The altitude indicated for vertical profiles refers to the middle of the layer. Horizontal error bars display the uncertainties of the parameters. Vertical error bars indicate the altitude range used to calculate each data point. Broad classifications of the above-3 km dust layer and the below-3 km dust layer are shown in horizontal lines. Vertical dashed lines indicate the range of values obtained in dust source regions. The maximum value of k_{ext} reported in the literature for dust in source regions is above $0.8 \text{ m}^2 \text{ g}^{-1}$.

11



13

Figure 9. Altitude dependence of (a) the fine mode effective diameter $D_{eff,f}$ (size range 0.053-1 μm) and (b) the coarse mode effective diameter $D_{eff,c}$ (size range 1-20 μm). The altitude reported for vertical profiles refers to the middle of the layer. Broad classifications of the above-3 km dust layer, the below-3 km dust layer and the boundary layer have been added to the figure.



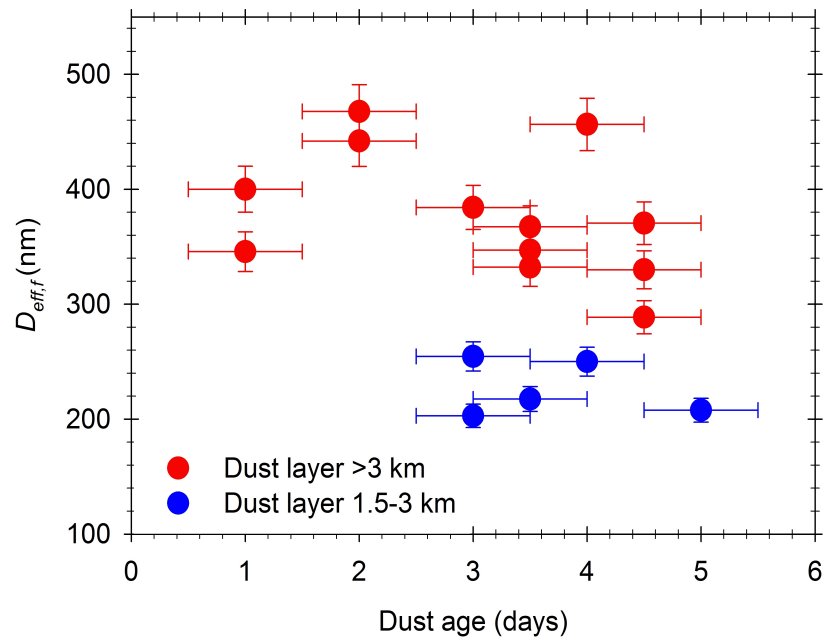
6

7

1

2

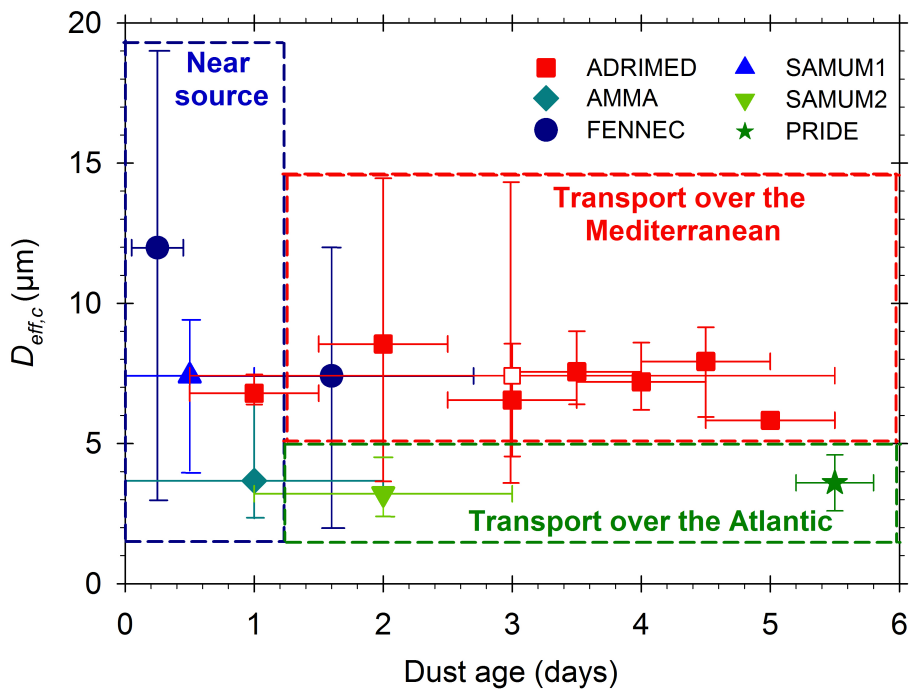
1Figure 10. Effective diameter of the fine mode D_{eff} as a function of the dust age observed for
2the above-3km dust layers (red circles) and the below-3km dust layers (blue circles).



4

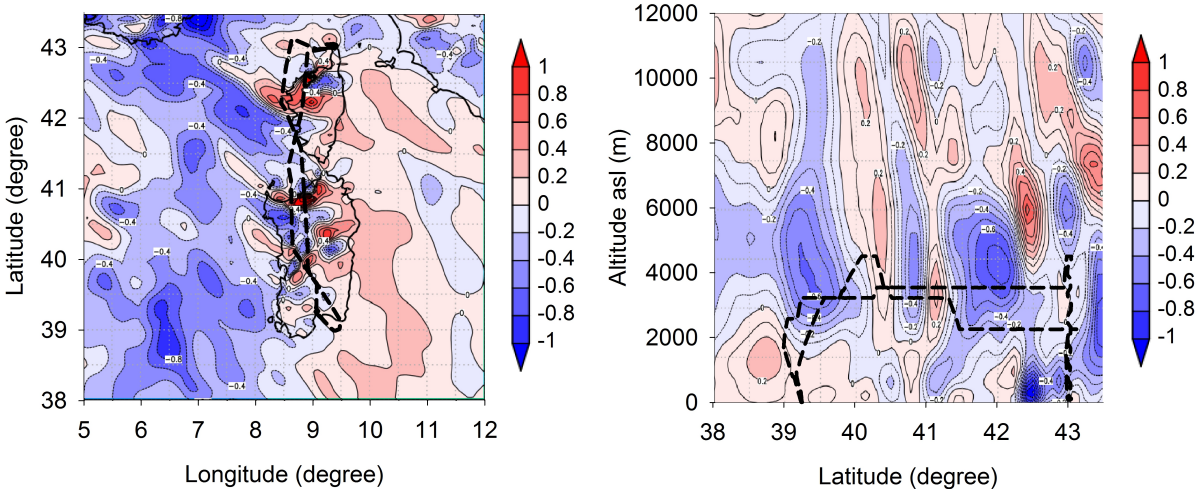
1Figure 11. Effective diameter of the coarse mode $D_{eff,c}$ as a function of the dust age observed
 2during ADRIMED (squares). Filled red squares represent the average values observed for
 3each dust age and the empty red square represents the campaign average value. Values are
 4compared to those observed in dust source region (in blue) during FENNEC (circles),
 5SAMUM1 (triangle) and AMMA (diamond), as well as measurements in the Atlantic Ocean
 6(in green) at Cape-Verde region during SAMUM-2 (triangle) and at Puerto-Rico during
 7PRIDE (stars). The horizontal error bars represent ± 0.5 -day uncertainties on the dust age
 8estimated using HYSPLIT and Sevir RGB images. The vertical error bars represent the range
 9of values obtained for each dust age.

10



12

1Figure 12. Wind vertical velocity (in Pa s^{-1}) at 700 hPa (a) and on the vertical along the F33
2flight latitude (b), from the 10-km resolution WRF model simulations. The dashed line shows
3the flight track.



5

1References

- 2 Alados-Arboledas, L., Müller, D., Guerrero-Rascado, J. L., Navas-Guzman, D., Pérez-
3Ramirez, D., and Olmo, F. J.: Optical and microphysical properties of fresh biomass burning
4aerosol retrieved by Raman lidar, and star-and sun-photometry, *Geophys. Res. Lett.*, 38,
5L01807, doi:10.1029/2010GL45999, 2011.
- 6 Andreae, M. O., and Merlet, P.: Emission of trace gases and aerosols from biomass
7burning, *Global Biogeochem. Cy.*, 15, 955-966, doi:10.1029/2000GB001382, 2001.
- 8 Andreae, M. O., and Rosenfeld, D.: Aerosol-cloud-precipitation interactions. Part 1. The
9nature and sources of cloud-active aerosols, *Earth-Sci. Rev.*, 89, 13-41,
10doi:10.1016/j.earscirev.2008.03.001, 2008.
- 11 Ansmann, A., Baars, H., Tesche, M., Müller, D., Althausen, D., Engelmann, R.,
12Pauliquevis, T., and Artaxo, P.: Dust and smoke transport from Africa to South America: Lidar
13profiling over Cape Verde and the Amazon rainforest, *Geophys. Res. Lett.*, 36, L11802,
14doi:10.1029/2009GL037923, 2009.
- 15 Balkanski, Y., Schulz, M., Claquin, T., and Guibert, S.: Reevaluation of Mineral aerosol
16radiative forcings suggests a better agreement with satellite and AERONET data, *Atmos.*
17*Chem. Phys.*, 7, 81-95, doi:10.5194/acp-7-81-2007, 2007.
- 18 Basart, S., Pérez, C., Cuevas, E., Baldasano, J. M., and Gobbi, G. P.: Aerosol
19characterization in Northern Africa, Northeastern Atlantic, Mediterranean Basin and Middle
20East from direct-sun AERONET observations, *Atmos. Chem. Phys.*, 9, 8265-8282,
21doi:10.5194/acp-9-8265-2009, 2009.
- 22 Bauer, S.E., Balkanski, Y., Shulz, M., Hauglustaine, D. A., and Dentener F., Global
23modelling of heterogeneous chemistry on mineral aerosol surfaces: The influence of ozone
24chemistry and comparison to observations, *L. J. Geophys. Res.*, 109, D02304,
25doi:10.1029/2003JD003868, 2004.
- 26 Bauer, S. E., Mishchenko, M. I., Laci, A. A., Zhang, S., Perlwitz, J., and Metzger, S. M.:
27Do sulphate and nitrate coatings on mineral dust have important effects on radiative properties
28and climate modeling?, *J. Geophys. Res.*, 112, D06307, doi:10.1029/2005JD006977, 2007.
- 29 Baumgardner, D., Dye, J. E., Gandrud, B. W., and Knollenberg, R. G.: Interpretation of
30measurements made by forward scattering probe (FSSP-300) during the airborne arctic
31stratospheric expedition, *J. Geophys. Res.*, 97, 8035-8046, doi:10.1029/91JD02728, 1992.
- 32 Baumgardner, D., Popovicheva, O., Allan, J., Bernardoni, V., Cao, J., Cavalli, F., Cozic,
33J., Diapouli, E., Eleftheriadis, K., Genberg, P. J., Gonzalez, C., Gysel, M., John, A.,
34Kirchstetter, T. W., Kuhlbusch, T. A. J., Laborde, M., Lack, D., Müller, T., Niessner, R.,
35Petzold, A., Piazzalunga, A., Putaud, J. P., Schwarz, J., Sheridan, P., Subramanian, R.,
36Swietlicki, E., Valli, G., Vecchi, R., and Viana, M.: Soot reference materials for instrument
37calibration and intercomparisons: a workshop summary with recommendations, *Atmos. Meas.*
38*Techn.*, 5, 1869-1887, doi:10.5194/amt-5-1869-2012, 2012.
- 39 Bègue, N., Tulet, P., Chaboureau, J. P., Roberts, G., Gomes, L., and Mallet, M.: Long-
40range transport of Saharan dust over northwestern Europe during EUCAARI 2008 campaign:
41Evolution of dust optical properties by scavenging, *J. Geophys. Res.-Atmos.*, 117, D17201,
42doi:10.1029/2012jd017611, 2012.
- 43 Birmili, W., Heinke, K., Pitz, M., Matschullat, J., Wiedensohler, A., Cyrus, J., Wichmann,
44H. E., and Peters, A.: Particle number size distributions in urban air before and after
45volatilisation, *Atmos. Chem. Phys.*, 10, 4643-4660, doi:10.5194/acp-10-4643-2010, 2010.
- 46 Bohren, C. F., and Huffman, D. R.: Absorption and scattering of light by small particles,
47Wiley, New York, 1983.
- 48 Bove, M. C., Brotto, P., Cassola, F., Cuccia, E., Massabò, D., Mazzino, A., Piazzalunga,
49A., and Prati, P.: An integrated PM_{2.5} source apportionment study: Positive Matrix

1Factorization vs. the Chemical Transport Model CAMx, *Atmos. Environ.*, 94, 274-286,
2doi:10.1016/j.atmosenv.2014.05.039, 2014.

3 Cai, Y., Montague, D. C., Mooiweer-Bryan, W., and Deshler, T.: Performance
4characteristics of the ultra high sensitivity aerosol spectrometer for particles between 55 and
5800 nm: Laboratory and field studies, *J. Aerosol Sci.*, 39, 759-769,
6doi:10.1016/j.jaerosci.2008.04.007, 2008.

7 Cassola, F., Ferrari, F., Mazzino, and Mazzino, A.: Numerical simulations of
8Mediterranean heavy precipitation events with the WRF model: A verification exercise using
9different approaches, *Atmos. Res.*, 164-165, 210-225, doi:10.1016/j.atmosres.2015.05.010,
102015.

11 Charlson, R. J., Schwartz, S. E., Hales, J. M., Cess, R. D., Coakley, J. A., Hansen, J. E.,
12and Hofmann, D. J.: Climate forcing by anthropogenic aerosols, *Science*, 255, 423-430,
13doi:10.1126/science.255.5043.423, 1992.

14 Choobari, O. A., Zawar-Reza, P., and Sturman, A.: The global distribution of mineral dust
15and its impacts on the climate system: A review, *Atmos. Res.*, 138, 152-165,
16doi:10.1016/j.atmosres.2013.11.007, 2014.

17 Chou, C., Formenti, P., Maille, M., Ausset, P., Helas, G., Harrison, M., and Osborne, S.:
18Size distribution, shape, and composition of mineral dust aerosols collected during the African
19Monsoon Multidisciplinary Analysis Special Observation Period 0: Dust and Biomass-
20Burning Experiment field campaign in Niger, January 2006, *J. Geophys. Res.*, 113, D00C10,
21doi:10.1029/2008JD009897, 2008.

22 Clarke, A. D., Shinozuka, Y., Kapustin, V. N., Howell, S., Huebert, B., Doherty, S.,
23Anderson, T., Covert, D., Anderson, J., Hua, X., Moore, K. G., McNaughton, C., Carmichael,
24G., and Weber, R.: Size distributions and mixtures of dust and black carbon aerosol in Asian
25outflow: Physiochemistry and optical properties, *J. Geophys. Res.*, 109, D15S09,
26doi:10.1029/2003JD004378, 2004.

27 Collaud Coen, M., Weingartner, E., Schaub, D., Hueglin, C., Corrigan, C., Henning, S.,
28Schwikowski, M., and Baltensperger, U.: Saharan dust events at the Jungfraujoch: detection
29by wavelength dependence of the single scattering albedo and first climatology analysis,
30*Atmos. Chem. Phys.*, 4, 2465-2480, doi:10.5194/acp-4-2465-2004, 2004.

31 Crumeyrolle, S., Gomes, L., Tulet, P., Matsuki, A., Schwarzenboeck, A., and Crahan, K.:
32Increase of the aerosol hygroscopicity by cloud processing in a mesoscale convective system:
33a case study from the AMMA campaign, *Atmos. Chem. Phys.*, 8, 6907-6924,
34doi:10.5194/acp-8-6907-2008, 2008.

35 Cuesta, J., Marsham, J. H., Parker, D. J., and Flamant, C.: Dynamical mechanisms
36controlling the vertical redistribution of dust and the thermodynamic structure of the West
37Saharan atmospheric boundary layer during summer, *Atmos. Sci. Lett.*, 10, 34-42,
38doi:10.1002/asl.207, 2009.

39 d'Almeida, G. A.: A Model for Saharan Dust Transport, *J. Clim. Appl. Meteor.*, 25, 903-
40916, doi:10.1175/1520-0450(1986)025<0903:AMFSDT>2.0.CO;2, 1986.

41 DeCarlo, P., Slowik, J., Worsnop, D., Davidovits, P., & Jimenez, J.: Particle Morphology
42and Density Characterization by Combined Mobility and Aerodynamic Diameter
43Measurements. Part 1: Theory, *Aerosol Sci. Tech.*, 38, 1185-1205, doi:
4410.1080/027868290903907, 2004.

45 de Meij, A., and Lelieveld, J.: Evaluating aerosol optical properties observed by ground-
46based and satellite remote sensing over the Mediterranean and the Middle East in 2006,
47*Atmos. Res.*, 99, 415-433, doi:10.1016/j.atmosres.2010.11.005, 2011.

48 Di Biagio, C., di Sarra, A., Meloni, D., Monteleone, F., Piacentino, S., and Sferlazzo, D.:
49Measurements of Mediterranean aerosol radiative forcing and influence of the single
50scattering albedo, *J. Geophys. Res.*, 114, D06211, doi:10.1029/2008JD011037, 2009.

- 1 Di Biagio, C., Doppler, L., Gaimoz, C., Grand, N., Ancellet, G., Raut, J. C., Beekmann,
2M., Borbon, A., Sartelet, K., Attié, J. L., Ravetta, F., and Formenti, P.: Continental pollution in
3the Western Mediterranean Basin: vertical profiles of aerosol and trace gases measured over
4the sea during TRAQA 2012 and SAFMED 2013, *Atmos. Chem. Phys. Discuss.*, 15, 8283-
58328, doi:10.5194/acpd-15-8283-2015, 2015.
- 6 Di Iorio, T., di Sarra, A., Sferlazzo, D. M., Cacciani, M., Meloni, D., Monteleone, F., Fuà,
7D., and Fiocco, G.: Seasonal evolution of the tropospheric aerosol vertical profile in the
8central Mediterranean and role of desert dust, *J. Geophys. Res.*, 114, D02201,
9doi:10.1029/2008JD010593, 2009.
- 10 Doherty, O. M., Riemer, N., and Hameed, S.: Saharan mineral dust transport into the
11Caribbean: Observed atmospheric controls and trends, *J. Geophys. Res.*, 113, D07211,
12doi:10.1029/2007jd009171, 2008.
- 13 Draxler, R. R., and Rolph, G. D.: HYSPLIT (HYbrid Single-Particle Lagrangian
14Integrated Trajectory) Model access via NOAA ARL READY Website
15(<http://ready.arl.noaa.gov/HYSPLIT.php>). , NOAA Air Resources Laboratory, Silver Spring,
16MD, 2015.
- 17 Dulac, F., Bergametti, G., Losno, R., Remoudaki, E., Gomes, L., Ezat, U., and
18BuatMénard, P.: Dry deposition of mineral aerosol particles in the marine atmosphere:
19significance of the large size fraction, in: *Precipitation Scavenging and Atmosphere–Surface*
20*Exchange*, Schwartz, S. E. and Slinn, W. G. N., Hemisphere, Richland, Wa, 841–854, 1992
- 21 Dulac, F., and Chazette, P.: Airborne study of a multi-layer aerosol structure in the eastern
22Mediterranean observed with the airborne polarized lidar ALEX during a STAAARTE
23campaign (7 June 1997), *Atmos. Chem. Phys.*, 3, 1817-1831, doi:10.5194/acp-3-1817-2003,
242003.
- 25 Engelstaedter, S., Tegen, I., and Washington, R.: North African dust emissions and
26transport, *Earth-Sci. Rev.*, 79, 73-100, doi:10.1016/j.earscirev.2006.06.004, 2006.
- 27 Environmental Modeling Center: The GFS Atmospheric Model. NCEP Office Note 442.
28National Oceanic and Atmospheric Administration, 2003.
- 29 Fan, X.-B., Okada, K., Niimura, N., Kai, K., Arao, K., Shi, G.-Y., Qin, Y., and Mitsuta, Y.:
30Mineral particles collected in china and japan during the same Asian dust-storm event, *Atmos.*
31*Environ.*, 30, 347-351, doi:10.1016/1352-2310(95)00271-Y, 1996.
- 32 Flamant, C., Chaboureaud, J. P., Parker, D. J., Taylor, C. M., Cammas, J. P., Bock, O.,
33Timouk, F., and Pelon, J.: Airborne observations of the impact of a convective system on the
34planetary boundary layer thermodynamics and aerosol distribution in the inter-tropical
35discontinuity region of the West African Monsoon, *Q. J. Roy. Meteor. Soc.*, 133, 1175-1189,
36doi:10.1002/qj.97, 2007.
- 37 Formenti, P., Andreae, M. O., Lange, L., Roberts, G., Cafmeyer, J., Rajta, I., Maenhaut,
38W., Holben, B. N., Artaxo, P., and Lelieveld, J.: Saharan dust in Brazil and Suriname during
39the Large-Scale Biosphere-Atmosphere Experiment in Amazonia (LBA) - Cooperative LBA
40Regional Experiment (CLAIRE) in March 1998, *J. Geophys. Res.*, 106, 14919-14934,
41doi:10.1029/2000JD900827, 2001.
- 42 Formenti, P., Elbert, W., Maenhaut, W., Haywood, J., and Andreae, M. O.: Chemical
43composition of mineral dust aerosol during the Saharan Dust Experiment (SHADE) airborne
44campaign in the Cape Verde region, September 2000, *J. Geophys. Res.*, 108, 8576,
45doi:10.1029/2002JD002648, 2003.
- 46 Formenti, P., Rajot, J. L., Desboeufs, K., Caquineau, S., Chevaillier, S., Nava, S.,
47Gaudichet, A., Journet, E., Triquet, S., Alfaro, S., Chiari, M., Haywood, J., Coe, H., and
48Highwood, E.: Regional variability of the composition of mineral dust from western Africa:
49Results from the AMMA SOP0/DABEX and DODO field campaigns, *J. Geophys. Res.*, 113,
50D00C13, doi:10.1029/2008JD009903, 2008.

1 Formenti, P., Rajot, J. L., Desboeufs, K., Saïd, F., Grand, N., Chevaillier, S., and
2 Schmechtig, C.: Airborne observations of mineral dust over western Africa in the summer
3 Monsoon season: spatial and vertical variability of physico-chemical and optical properties,
4 *Atmos. Chem. Phys.*, 11, 6387-6410, doi:10.5194/acp-11-6387-2011, 2011a.

5 Formenti, P., Schütz, L., Balkanski, Y., Desboeufs, K., Ebert, M., Kandler, K., Petzold, A.,
6 Scheuvs, D., Weinbruch, S., and Zhang, D.: Recent progress in understanding physical and
7 chemical properties of African and Asian mineral dust, *Atmos. Chem. Phys.*, 11, 8231-
8 8256, doi:10.5194/acp-11-8231-2011, 2011b.

9 Formenti, P., Caquineau, S., Desboeufs, K., Klaver, A., Chevaillier, S., Journet, E., and
10 Rajot, J. L.: Mapping the physico-chemical properties of mineral dust in western Africa:
11 mineralogical composition, *Atmos. Chem. Phys.*, 14, 10663-10686, doi:10.5194/acp-14-
12 10663-2014, 2014.

13 Garrett, T. J., Russell, L. M., Ramaswamy, V., Maria, S. F., and Huebert, B. J.:
14 Microphysical and radiative evolution of aerosol plumes over the tropical North Atlantic
15 Ocean, *J. Geophys. Res.*, 108, 4022, doi:10.1029/2002JD002228, 2003.

16 Gkikas, A., Houssos, E. E., Hatzianastassiou, N., Papadimas, C. D., and Bartzokas, A.:
17 Synoptic conditions favouring the occurrence of aerosol episodes over the broader
18 Mediterranean basin, *Q. J. Roy. Meteor. Soc.*, 138, 932-949, doi:10.1002/qj.978, 2012.

19 Ginoux, P., J. M. Prospero, T. E. Gill, N. C. Hsu, and M. Zhao (2012), Global-scale
20 attribution of anthropogenic and natural dust sources and their emission rates based on
21 MODIS Deep Blue aerosol products, *Rev. Geophys.*, 50, RG3005,
22 doi:10.1029/2012RG000388, 2012.

23 Gobbi, G. P., Barnada, F., Giorgi, R., and Santacasa, A.: Altitude-resolved properties of a
24 Saharan dust event over the Mediterranean, *Atmos. Environ.*, 34, 5119-5127, 2000.

25 Gomes, L., Bergametti, G., Coudé-Gaussen, G., and Rognon, P.: Submicron desert dusts:
26 a sandblasting process, *J. Geophys. Res.*, 95, 13927-13935, doi:10.1029/JD095iD09p13927,
27 1990.

28 Gómez-Amo, J. L., Pinti, V., Di Iorio, T., di Sarra, A., Meloni, D., Becagli, S., Bellantone,
29 V., Cacciani, M., Fuà, D., and Perrone, M. R.: The June 2007 Saharan dust event in the central
30 Mediterranean: Observations and radiative effects in marine, urban, and sub-urban
31 environments, *Atmos. Environ.*, 45, 5385-5393,
32 <http://dx.doi.org/10.1016/j.atmosenv.2011.06.045>, 2011.

33 Goudie, A. S., and Middleton, N. J.: Saharan dust storms: nature and consequences,
34 *Earth-Sci. Rev.*, 56, 179-204, doi:10.1016/S0012-8252(01)00067-8, 2001.

35 Guerrero-Rascado, J. L., Ruiz, B., and Alados-Arboledas, L.: Multi-spectral Lidar
36 characterization of the vertical structure of Saharan dust aerosol over southern Spain, *Atmos.*
37 *Environ.*, 42, 2668-2681, <http://dx.doi.org/10.1016/j.atmosenv.2007.12.062>, 2008.

38 Guieu, C., Loye-Pilot, M. D., Ridame, C., and Thomas, C.: Chemical characterization of
39 the Saharan dust end-member: Some biogeochemical implications for the western
40 Mediterranean Sea, *J. Geophys. Res.*, 107, 4258, doi:10.1029/2001JD000582, 2002.

41 Hamonou, E., Chazette, P., Balis, D., Dulac, F., Schneider, X., Galani, E., Ancellet, G.,
42 and Papayannis, A.: Characterization of the vertical structure of Saharan dust export to the
43 Mediterranean basin, *J. Geophys. Res.*, 104, 22257-22270, doi:10.1029/1999JD900257, 1999.

44 Haywood, J. M., Johnson, B. T., Osborne, S. R., Baran, A. J., Brooks, M., Milton, S. F.,
45 Mulcahy, J., Walters, D., Allan, R. P., Klaver, A., Formenti, P., Brindley, H. E., Christopher,
46 S., and Gupta, P.: Motivation, rationale and key results from the GERBILS Saharan dust
47 measurement campaign, *Q. J. Roy. Meteor. Soc.*, 137, 1106-1116, doi:10.1002/qj.797, 2011.

48 Heintzenberg, J.: The SAMUM-1 experiment over Southern Morocco: overview and
49 introduction, *Tellus B*, 61, 2-11, doi:10.1111/j.1600-0889.2008.00403.x, 2009.

- 1 Hess, M., Koepke, P., and Schult, I.: Optical Properties of Aerosols and Clouds: The
2Software Package OPAC, *B. Am. Meteorol. Soc.*, 79, 831-844, doi:10.1175/1520-
30477(1998)079<0831:OPOAAC>2.0.CO;2, 1998.
- 4 Hinds, W. C.: *Aerosol Technology: Properties, Behavior, and Measurement of Airborne*
5*Particles*, 2nd Ed.. Wiley, New York, 1999.
- 6 Huneus, N., Chevallier, F., and Boucher, O.: Estimating aerosol emissions by
7assimilating observed aerosol optical depth in a global aerosol model, *Atmos. Chem. Phys.*,
812, 4585-4606, doi:10.5194/acp-12-4585-2012, 2012.
- 9 IPCC, fifth assessment report - the physical science basis, <http://www.ipcc.ch>, 2013.
- 10 Jing, S., Jianping, H., Qiang, F., Minnis, P., Jinming, G., and Jianrong, B.: Estimation of
11Asian dust aerosol effect on cloud radiation forcing using Fu-Liou radiative model and
12CERES measurements, *Atmos. Chem. Phys.*, 8, 2763-2771, doi:10.5194/acp-8-2763-2008,
132008.
- 14 Junkermann, W.: On the distribution of formaldehyde in the western Po-Valley, Italy,
15during FORMAT 2002/2003, *Atmos. Chem. Phys.*, 9, 9187-9196, doi:10.5194/acp-9-9187-
162009, 2009.
- 17 Kaaden, N., Massling, A., Schladitz, A., Muller, T., Kandler, K., Schutz, L., Weinzierl, B.,
18Petzold, A., Tesche, M., Leinert, S., Deutscher, C., Ebert, M., Weinbruch, S., and
19Wiedensohler, A.: State of mixing, shape factor, number size distribution, and hygroscopic
20growth of the Saharan anthropogenic and mineral dust aerosol at Tinfou, Morocco, *Tellus B*,
2161, 51-63, doi:10.1111/j.1600-0889.2008.00388.x, 2009.
- 22 Kalashnikova, O. V., and Kahn, R. A.: Mineral dust plume evolution over the Atlantic
23from MISR and MODIS aerosol retrievals, *J. Geophys. Res.*, 113, D24204,
24doi:10.1029/2008JD010083, 2008.
- 25 Kalnay, E., Kanamitsu, M., Kistler, R., Collins, W., Deaven, D., Gandin, L., Iredell, M.,
26Saha, S., White, G., Woollen, J., Zhu, Y., Leetmaa, A., Reynolds, R., Chelliah, M., Ebisuzaki,
27W., Higgins, W., Janowiak, J., Mo, K. C., Ropelewski, C., Wang, J., Jenne, R., and Joseph, D.:
28The NCEP/NCAR 40-Year Reanalysis Project, *B. Am. Meteorol. Soc.*, 77, 437-471,
29doi:10.1175/1520-0477(1996)077<0437:TNYRP>2.0.CO;2, 1996.
- 30 Kandler, K., SchÜTz, L., Deutscher, C., Ebert, M., Hofmann, H., JÄCkel, S., Jaenicke,
31R., Knippertz, P., Lieke, K., Massling, A., Petzold, A., Schladitz, A., Weinzierl, B.,
32Wiedensohler, A., Zorn, S., and Weinbruch, S.: Size distribution, mass concentration,
33chemical and mineralogical composition and derived optical parameters of the boundary layer
34aerosol at Tinfou, Morocco, during SAMUM 2006, *Tellus B*, 61, 32-50, doi:10.1111/j.1600-
350889.2008.00385.x, 2009.
- 36 Kanitz, T., Engelmann, R., Heinold, B., Baars, H., Skupin, A., and Ansmann, A.: Tracking
37the Saharan Air Layer with shipborne lidar across the tropical Atlantic, *Geophys. Res. Lett.*,
3841, 1044-1050, doi:10.1002/2013GL058780, 2014.
- 39 Kaufman, Y. J., Tanré, D., Dubovik, D. O., Karnieli, A., and Remer, L. A.: Absorption of
40sunlight by dust as inferred from satellite and ground-based remote sensing, *Geophys. Res.*
41*Lett.*, 28, 1479-1482, 2001.
- 42 Koçak, M., Theodosi, C., Zarrmpas, P., Séguret, M. J. M., Herut, B., Kallos, G.,
43Mihalopoulos, N., Kubilay, N., and Nimmo, M.: Influence of mineral dust transport on the
44chemical composition and physical properties of the Eastern Mediterranean aerosol, *Atmos.*
45*Environ.*, 57, 266-277, <http://dx.doi.org/10.1016/j.atmosenv.2012.04.006>, 2012.
- 46 Koehler, K. A., Kreidenweis, S. M., DeMott, P. J., Petters, M. D., Prenni, A. J., and
47Carrico, C. M.: Hygroscopicity and cloud droplet activation of mineral dust aerosol, *Geophys.*
48*Res. Lett.*, 36, L08805, doi:10.1029/2009GL037348, 2009.
- 49 Korhonen, H., Napari, I., Timmreck, C., Vehkamäki, H., Pirjola, L., Lehtinen, K. E. J.,
50Lauri, A., and Kulmala, M.: Heterogeneous nucleation as a potential sulphate-coating

1 mechanism of atmospheric mineral dust particles and implications of coated dust on new
2 particle formation, *J. Geophys. Res.*, 108, 4546, doi:10.1029/2003JD003553, 2003.

3 Koren, I., Joseph, J. H., and Israelevich, P.: Detection of dust plumes and their sources in
4 northeastern Libya, *Can. J. Remote Sens.*, 29, 792-796, doi:10.5589/m03-036, 2003.

5 Kutuzov, S., Shahgedanova, M., Mikhalevko, V., Ginot, P., Lavrentiev, I., and Kemp, S.:
6 High-resolution provenance of desert dust deposited on Mt. Elbrus, Caucasus in 2009-2012
7 using snow pit and firn core records, *The Cryosphere*, 7, 1481-1498, doi:10.5194/tc-7-1481-
8 2013, 2013.

9 Laborde, M., Mertes, P., Zieger, P., Dommen, J., Baltensperger, U., and Gysel, M.:
10 Sensitivity of the Single Particle Soot Photometer to different black carbon types, *Atmos.*
11 *Meas. Tech.*, 5, 1031-1043, doi:10.5194/amt-5-1031-2012, 2012.

12 Lack, D. A., and Cappa, C. D.: Impact of brown and clear carbon on light absorption
13 enhancement, single scatter albedo and absorption wavelength dependence of black carbon,
14 *Atmos. Chem. Phys.*, 10, 4207-4220, doi:10.5194/acp-10-4207-2010, 2010.

15 Levin, Z., Ganor, E., and Gladstein, V.: The Effects of Desert Particles Coated with
16 Sulfate on Rain Formation in the Eastern Mediterranean, *J. Appl. Meteor.*, 35, 1511-1523,
17 doi:10.1175/1520-0450(1996)035<1511:TEODPC>2.0.CO;2, 1996.

18 Levin, Z., Teller, A., Ganor, E., and Yin, Y.: On the interactions of mineral dust, sea-salt
19 particles, and clouds: A measurement and modeling study from the Mediterranean Israeli Dust
20 Experiment campaign, *J. Geophys. Res.*, 110, D20202, doi:10.1029/2005JD005810, 2005.

21 Liu, Y. G., and Daum, P. H.: Relationship of refractive index to mass density and self-
22 consistency of mixing rules for multicomponent mixtures like ambient aerosols, *J. Aerosol*
23 *Sci.*, 39, 974-986, doi:10.1016/j.jaerosci.2008.06.006, 2008.

24 Liu, D., Allan, J. D., Young, D. E., Coe, H., Beddows, D., Fleming, Z. L., Flynn, M. J.,
25 Gallagher, M. W., Harrison, R. M., Lee, J., Prevot, A. S. H., Taylor, J. W., Yin, J., Williams, P.
26 I., and Zotter, P.: Size distribution, mixing state and source apportionment of black carbon
27 aerosol in London during wintertime, *Atmos. Chem. Phys.*, 14, 10061-10084, doi:10.5194/acp-
28 2814-10061-2014, 2014.

29 Ma, Q. X., Liu, Y. C., Liu, C., and He, H.: Heterogeneous reaction of acetic acid on MgO,
30 α -Al₂O₃, and CaCO₃ and the effect on the hygroscopic behaviour of these particles,
31 *Phys. Chem. Chem. Phys.*, 14, 8403-8409, doi:10.1039/c2cp40510e, 2012.

32 Mahowald, N., Albani, S., Kok, J. F., Engelstaeder, S., Scanza, R., Ward, D. S., and
33 Flanner, M. G.: The size distribution of desert dust aerosols and its impact on the Earth
34 system, *Aeolian Research*, 15, 53-71, doi:10.1016/j.aeolia.2013.09.002, 2014.

35 Mallet, M., Van Dingenen, R., Roger, J. C., Despiiau, S., and Cachier, H.: In situ airborne
36 measurements of aerosol optical properties during photochemical pollution events, *J.*
37 *Geophys. Res.*, 110, doi:10.1029/2004jd005139, 2005.

38 Mallet, M., Dubovik, O., Nabat, P., Dulac, F., Kahn, R., Sciare, J., Paronis, D., and Léon,
39 J. F.: Absorption properties of Mediterranean aerosols obtained from multi-year ground-based
40 remote sensing observations, *Atmos. Chem. Phys.*, 13, 9195-9210, doi:10.5194/acp-13-9195-
41 412013, 2013.

42 Mallet, M., Dulac, F., Formenti, P., Nabat, P., Sciare, J., Roberts, G., Pelon, J., Ancellet,
43 G., Tanré, D., Parol, F., di Sarra, A., Alados, L., Arndt, J., Auriol, F., Blarel, L., Bourrianne, T.,
44 Brogniez, G., Chazette, P., Chevaillier, S., Claeys, M., D'Anna, B., Denjean, C., Derimian, Y.,
45 Desboeufs, K., Di Iorio, T., Doussin, J. F., Durand, P., Féron, A., Freney, E., Gaimoz, C.,
46 Goloub, P., Gómez-Amo, J. L., Granados-Muñoz, M. J., Grand, N., Hamonou, E., Jankowiak,
47 I., Jeannot, M., Léon, J. F., Maillé, M., Mailler, S., Meloni, D., Menut, L., Momboisse, G.,
48 Nicolas, J., Podvin, J., Pont, V., Rea, G., Renard, J. B., Roblou, L., Schepanski, K.,
49 Schwarzenboeck, A., Sellegri, K., Sicard, M., Solmon, F., Somot, S., Torres, B., Totems, J.,
50 Triquet, S., Verdier, N., Verwaerde, C., Wenger, J., and Zapf, P.: Overview of the Chemistry-
51 Aerosol Mediterranean Experiment/Aerosol Direct Radiative Forcing on the Mediterranean

- 1Climate (ChArMEx/ADRI-MED) summer 2013 campaign, *Atmos. Chem. Phys. Discuss.*, 15, 219615-19727, doi:10.5194/acpd-15-19615-2015, 2015.
- 3 Mantas, E., Remoundaki, E., Halari, I., Kassomenos, P., Theodosi, C., Hatzikioseyan, A.,
4and Mihalopoulos, N.: Mass closure and source apportionment of PM_{2.5} by Positive Matrix
5Factorization analysis in urban Mediterranean environment, *Atmos. Environ.*, 94, 154-163,
6doi:10.1016/j.atmosenv.2014.05.002, 2014.
- 7 Marconi, M., Sferlazzo, D. M., Becagli, S., Bommarito, C., Calzolari, G., Chiari, M., di
8Sarra, A., Ghedini, C., Gómez-Amo, J. L., Lucarelli, F., Meloni, D., Monteleone, F., Nava, S.,
9Pace, G., Piacentino, S., Rugi, F., Severi, M., Traversi, R., and Udisti, R.: Saharan dust aerosol
10over the central Mediterranean Sea: PM₁₀ chemical composition and concentration versus
11optical columnar measurements, *Atmos. Chem. Phys.*, 14, 2039-2054, doi:10.5194/acp-14-
122039-2014, 2014.
- 13 Maring, H., Savoie, D. L., Izaguirre, M. A., Custals, L., and Reid, J. S.: Mineral dust
14aerosol size distribution change during atmospheric transport, *J. Geophys. Res.*, 108, 8592,
15doi:10.1029/2002jd002536, 2003.
- 16 Massoli, P., Kebejian, P. L., Onasch, T. B., Hills, F. B., and Freedman, A., Aerosol light
17extinction measurements by Cavity Attenuated Phase Shift (CAPS) Spectroscopy: Laboratory
18validation and field deployment of a compact aerosol particle extinction monitor, *Aerosol Sci.*
19*Tech.*, 428-435, doi:10.1080/02786821003716599, 2010.
- 20 McConnell, C. L., Highwood, E. J., Coe, H., Formenti, P., Anderson, B., Osborne, S.,
21Nava, S., Desboeufs, K., Chen, G., and Harrison, M. A. J.: Seasonal variations of the physical
22and optical characteristics of Saharan dust: Results from the Dust Outflow and Deposition to
23the Ocean (DODO) experiment, *J. Geophys. Res.*, 113, D14505, doi:10.1029/2007jd009606,
242008.
- 25 Meloni, D., di Sarra, A., DeLuisi, J., Di Iorio, T., Fiocco, G., Junkermann, W., and Pace,
26G.: Tropospheric aerosols in the Mediterranean: 2. Radiative effects through model
27simulations and measurements, *J. Geophys. Res.*, 108, 4317, doi:10.1029/2002JD002807,
282003.
- 29 Meloni, D., di Sarra, A., Pace, G., and Monteleone, F.: Aerosol optical properties at
30Lampedusa (Central Mediterranean). 2. Determination of single scattering albedo at two
31wavelengths for different aerosol types, *Atmos. Chem. Phys.*, 6, 715-727, doi:10.5194/acp-6-
32715-2006, 2006.
- 33 Mentaschi, L., Besio, G., Cassola, F., and Mazzino, A.: Performance evaluation of
34WavewatchIII in the Mediterranean Sea, *Ocean Model.*, 90, 82-94,
35doi:10.1016/j.ocemod.2015.04.003, 2015.
- 36 Mian Chin, Diehl, T., Dubovick, O., Eck, T. F., Holben, B. N., Sinyiuk, A., and Streets, D.
37G.: Light absorption by pollution, dust, and biomass burning aerosols: a global model study
38and evaluation with AERONET measurements, *Ann. Geophys.*, 27, 3439-3464,
39doi:10.5194/angeo-27-3439-2009, 2009.
- 40 Mishchenko, M. I., Lasis, A. A., Carlson, B. E., and Travis, L. D. : Nonsphericity of dust-
41like tropospheric aerosols : implications for aerosol remote sensing and climate modelling,
42*Geophys. Res. Lett.*, 1077-1080, 1995.
- 43 Mona, L., Amodeo, A., Pandolfi, M., and Pappalardo, G.: Saharan dust intrusions in the
44Mediterranean area: Three years of Raman lidar measurements, *J. Geophys. Res.*, 111,
45D16203, doi:10.1029/2005JD006569, 2006.
- 46 Moteki, N., and Kondo, Y.: Dependence of Laser-Induced Incandescence on Physical
47Properties of Black Carbon Aerosols: Measurements and Theoretical Interpretation, *Aerosol*
48*Sci. Tech.*, 44, 663-675, doi:10.1080/02786826.2010.484450, 2010.
- 49 Moulin, C., Lambert, C. E., Dulac, F., and Dayan, U.: Control of atmospheric export of
50dust from North Africa by the North Atlantic Oscillation, *Nature*, 387, 691-694, 1997.

1 Moulin, C., Lambert, C. E., Dayan, U., Masson, V., Ramonet, M., Bousquet, P., Legrand,
2M., Balkanski, Y. J., Guelle, W., Marticorena, B., Bergametti, G., and Dulac, F.: Satellite
3climatology of African dust transport in the Mediterranean atmosphere, *J. Geophys. Res.*, 103,
413137-13144, doi:10.1029/98JD00171, 1998.

5 Moulin, C., Gordon, H. R., Banzon, V. F., and Evans, R. H.: Assessment of Saharan dust
6absorption in the visible from Sea- WiFS imagery, *J. Geophys. Res.*, 106(D16), 18 239–18
7250, doi:10.1029/2000JD900812, 2001.

8 Muller, T., Laborde, M., Kassell, G., and Wiedensohler, A.: Design and performance of a
9three-wavelength LED-based total scatter and backscatter integrating nephelometer, *Atmos.*
10*Meas. Tech.*, 4., 1291-1303, doi:10.5194/amt-4-1291-2011, 2011a.

11 Muller, T., Schladitz, A., Kandler, K., and Wiedensohler, A.: Spectral particle absorption
12coefficients, single scattering albedos and imaginary parts of refractive indices from ground
13based in situ measurements at Cape Verde Island during SAMUM-2, *Tellus B*, 63, 573-588,
14doi:10.1111/j.1600-0889.2011.00572.x, 2011b.

15 Nabat, P., Solmon, F., Mallet, M., Michou, M., Sevault, F., Driouech, F., Meloni, D., di
16Sarra, A., Di Biagio, C., Formenti, P., Sicard, M., Léon, J.-F., and Bouin, M. -N.: Dust aerosol
17radiative effects during summer 2012 simulated with a coupled regional aerosol-atmosphere-
18ocean model over the Mediterranean, *Atmos. Chem. Phys.*, 15, 3303-3326, doi:10.5194/acp-
1915-3303-2015, 2015.

20 Osborne, S. R., Johnson, B. T., Haywood, J. M., Baran, A. J., Harrison, M. A. J., and
21McConnell, C. L.: Physical and optical properties of mineral dust aerosol during the Dust and
22Biomass-burning Experiment, *J. Geophys. Res.*, 113, doi:10.1029/2007jd009551, 2008.

23 Otto, S., Bierwirth, E., Weinzierl, B., Kandler, K., Esselborn, M., Tesche, M., Schladitz,
24A., Wendisch, M., and Trautmann, T.: Solar radiative effects of a Saharan dust plume
25observed during SAMUM assuming spheroidal model particles, *Tellus B*, 61, 270-296,
26doi:10.1111/j.1600-0889.2008.00389.x, 2009.

27 Pace, G., Meloni, D., and di Sarra, A.: Forest fire aerosol over the Mediterranean basin
28during summer 2003, *J. Geophys. Res.*, 110, D21202, doi:10.1029/2005JD005986, 2005.

29 Papayannis, A., Amiridis, V., Mona, L., Tsaknakis, G., Balis, D., Bosenberg, J.,
30Chaikovski, A., De Tomasi, F., Grigorov, I., Mattis, I., Mitev, V., Muller, D., Nickovic, S.,
31Perez, C., Pietruczuk, A., Pisani, G., Ravetta, F., Rizi, V., Sicard, M., Trickl, T., Wiegner, M.,
32Gerding, M., Mamouri, R. E., D'Amico, G., and Pappalardo, G.: Systematic lidar observations
33of Saharan dust over Europe in the frame of EARLINET (2000-2002), *J. Geophys. Res.*, 113,
34D10204, doi:10.1029/2007jd009028, 2008.

35 Perrone, M. R., and Bergamo, A.: Direct radiative forcing during Sahara dust intrusions at
36a site in the Central Mediterranean: Anthropogenic particle contribution, *Atmos. Res.*, 101,
37783-798, doi:10.1016/j.atmosres.2011.05.011, 2011.

38 Perry, K. D., Cahill, T. A., Eldred, R. A., Dutcher, D. D., and Gill, T. E.: Long-range
39transport of North African dust to the eastern United States, *J. Geophys. Res.*, 102, 11225-
4011238, doi:10.1029/97JD00260, 1997.

41 Petzold, A., Rasp, K., Weinzierl, B., Esselborn, M., Hamburger, T., DÖRnbrack, A.,
42Kandler, K., SchÜTz, L., Knippertz, P., Fiebig, M., and Virkkula, A. K. I.: Saharan dust
43absorption and refractive index from aircraft-based observations during SAMUM 2006, *Tellus*
44*B*, 61, 118-130, doi:10.1111/j.1600-0889.2008.00383.x, 2009.

45 Pey, J., Querol, X., Alastuey, A., Forastiere, F., and Stafoggia, M.: African dust outbreaks
46over the Mediterranean Basin during 2001–2011: PM10 concentrations,
47phenomenology and trends, and its relation with synoptic and mesoscale meteorology, *Atmos.*
48*Chem. Phys.*, 13, 1395-1410,doi:10.5194/acp-13-1395-2013, 2013.

49 Prospero, J. M., Ginoux, P., Torres, O., Nicholson, S. E., and Gill, T. E.: Environmental
50characterization of global sources of atmospheric soil dust identified with the nimbus 7 total

lozone mapping spectrometer (TOMS) absorbing aerosol product, *Rev. Geophys.*, 40, 1002, doi:10.1029/2000RG000095, 2002.

3 Querol, X., Alastuey, A., Pey, J., Cusack, M., Pérez, N., Mihalopoulos, N., Theodosi, C.,
4 Gerasopoulos, E., Kubilay, N., and Koçak, M.: Variability in regional background aerosols
5 within the Mediterranean, *Atmos. Chem. Phys.*, 9, 4575-4591, doi:10.5194/acp-9-4575-2009,
6 2009.

7 Reid, J. S., Kinney, J. E., Westphal, D. L., Holben, B. N., Welton, E. J., Tsay, S.-C.,
8 Eleuterio, D. P., Campbell, J. R., Christopher, S. A., Colarco, P. R., Jonsson, H. H.,
9 Livingston, J. M., Maring, H. B., Meier, M. L., Pilewskie, P., Prospero, J. M., Reid, E. A.,
10 Remer, L. A., Russell, P. B., Savoie, D. L., Smirnov, A., and Tanré, D.: Analysis of
11 measurements of Saharan dust by airborne and ground-based remote sensing methods during
12 the Puerto Rico Dust Experiment (PRIDE), *J. Geophys. Res.*, 108, 8586,
13 doi:10.1029/2002JD002493, 2003.

14 Renard, J.-B. et al.: LOAC: a small aerosol optical counter/sizer for ground-based and
15 balloon measurements of the size distribution and nature of atmospheric particles – Part 2:
16 First results from balloon and unmanned aerial vehicle flights, *Atmos. Meas. Tech. Discuss.*,
17 178, 10057-10096, doi:10.5194/amtd-8-10057-2015, 2015.

18 Ripoll, A., Minguillón, M. C., Pey, J., Pérez, N., Querol, X., and Alastuey, A.: Joint
19 analysis of continental and regional background environments in the western Mediterranean:
20 PM₁ and PM₁₀ concentrations and composition, *Atmos. Chem. Phys.*, 15, 1129-
21 1145, doi:10.5194/acp-15-1129-2015, 2015.

22 Rosenberg, P. D., Parker, D. J., Ryder, C. L., Marsham, J. H., Garcia-Carreras, L., Dorsey,
23 J. R., Brooks, I. M., Dean, A. R., Crosier, J., McQuaid, J. B., and Washington, R.: Quantifying
24 particle size and turbulent scale dependence of dust flux in the Sahara using aircraft
25 measurements, *J. Geophys. Res.*, 119, 7577-7598, doi:10.1002/2013JD021255, 2014.

26 Rosenfeld, D., Rudich, Y., and Lahav, R.: Desert dust suppressing precipitation: A
27 possible desertification feedback loop, *P. Natl. Ac. Sci.*, 98, 5975-5980,
28 doi:10.1073/pnas.101122798, 2001.

29 Ryder, C. L., Highwood, E. J., Lai, T. M., Sodemann, H., and Marsham, J. H.: Impact of
30 atmospheric transport on the evolution of microphysical and optical properties of Saharan
31 dust, *Geophys. Res. Lett.*, 40, 2433-2438, doi:10.1002/grl.50482, 2013a.

32 Ryder, C. L., Highwood, E. J., Rosenberg, P. D., Trembath, J., Brooke, J. K., Bart, M.,
33 Dean, A., Crosier, J., Dorsey, J., Brindley, H., Banks, J., Marsham, J. H., McQuaid, J. B.,
34 Sodemann, H., and Washington, R.: Optical properties of Saharan dust aerosol and
35 contribution from the coarse mode as measured during the Fennec 2011 aircraft campaign,
36 *Atmos. Chem. Phys.*, 13, 303-325, doi:10.5194/acp-13-303-2013, 2013b.

37 Saha, A., Mallet, M., Roger, J. C., Dubuisson, P., Piazzola, J., and Despiiau, S.: One year
38 measurements of aerosol optical properties over an urban coastal site: Effect on local direct
39 radiative forcing, *Atmos. Res.*, 90, 195-202, doi:10.1016/j.atmosres.2008.02.003, 2008.

40 Saha, S., Moorthi, S., Pan, H.-L., Wu, X., Wang, J., Nadiga, S., Tripp, P., Kistler, R.,
41 Woollen, J., Behringer, D., Liu, H., Stokes, D., Grumbine, R., Gayno, G., Wang, J., Hou, Y.-
42 T., Chuang, H.-Y., Juang, H.-M. H., Sela, J., Iredell, M., Treadon, R., Kleist, D., Van Delst, P.,
43 Keyser, D., Derber, J., Ek, M., Meng, J., Wei, H., Yang, R., Lord, S., Van Den Dool, H.,
44 Kumar, A., Wang, W., Long, C., Chelliah, M., Xue, Y., Huang, B., Schemm, J.-K., Ebisuzaki,
45 W., Lin, R., Xie, P., Chen, M., Zhou, S., Higgins, W., Zou, C.-Z., Liu, Q., Chen, Y., Han, Y.,
46 Cucurull, L., Reynolds, R. W., Rutledge, G., and Goldberg, M.: The NCEP Climate Forecast
47 System Reanalysis, *B. Am. Meteorol. Soc.*, 91, 1015-1057, doi:10.1175/2010BAMS3001.1,
48 2010.

49 Saïd, F., Canut, G., Durand, P., Lohou, F., and Lothon, M.: Seasonal evolution of
50 boundary-layer turbulence measured by aircraft during the AMMA 2006 Special Observation
51 Period, *Q. J. Roy. Meteor. Soc.*, 136, 47-65, doi:10.1002/qj.475, 2010.

- 1 Salvador, P., Alonso-Pérez, S., Pey, J., Artíñano, B., de Bustos, J. J., Alastuey, A., and
2 Querol, X.: African dust outbreaks over the western Mediterranean Basin: 11-year
3 characterization of atmospheric circulation patterns and dust source areas, *Atmos. Chem.*
4 *Phys.*, 14, 6759-6775, doi:10.5194/acp-14-6759-2014, 2014.
- 5 Scheuvens, D., Schütz, L., Kandler, K., Ebert, M., and Weinbruch, S.: Bulk composition
6 of northern African dust and its source sediments — A compilation, *Earth-Sci. Rev.*, 116, 170-
7 194, doi:10.1016/j.earscirev.2012.08.005, 2013.
- 8 Schladitz, A., Müller, T., Kaaden, N., Massling, A., Kandler, K., Ebert, M., Weinbruch, S.,
9 Deutscher, C., and Wiedensohler, A.: In situ measurements of optical properties at Tinfou
10 (Morocco) during the Saharan Mineral Dust Experiment SAMUM 2006, *Tellus B*, 61, 64-78,
11 doi:10.1111/j.1600-0889.2008.00397.x, 2009.
- 12 Schladitz, A., Müller, T., Nordmann, S., Tesche, M., Groß, S., Freudenthaler, V.,
13 Gasteiger, J., and Wiedensohler, A.: In situ aerosol characterization at Cape Verde, *Tellus B*,
14 63, 549-572, doi:10.1111/j.1600-0889.2011.00568.x, 2011.
- 15 Seinfeld, J. H., and Pandis, S. N.: *Atmospheric chemistry and physics: From air pollution*
16 *to climate change*, 714 pp., 1998.
- 17 Sicard, M., Mallet, M., García-Vizcaíno, D., Comerón, A., Rocadenbosch, F., Dubuisson,
18 P., and Muñoz-Porcar, C.: Intense dust and extremely fresh biomass burning outbreak in
19 Barcelona, Spain: characterization of their optical properties and estimation of their direct
20 radiative forcing, *Environ. Res. Lett.*, 7, 034016, doi:10.1088/1748-9326/7/3/034016, 2012.
- 21 Sicard, M., Bertolín, S., Mallet, M., Dubuisson, P., and Comerón, A.: Estimation of
22 mineral dust long-wave radiative forcing: sensitivity study to particle properties and
23 application to real cases in the region of Barcelona, *Atmos. Chem. Phys.*, 14, 9213-
24 9231, doi:10.5194/acp-14-9213-2014, 2014.
- 25 Skamarock, W. C., Klemp, J. B., Dudhia, J., Gill, D. O., Barker, D. M., Huang, X. Z.,
26 Wang, W., and Powers, J. G.: *A Description of the Advanced Research WRF Version 3.*
27 *Technical report. Mesoscale and Microscale Meteorology Division, NCAR, Boulder,*
28 *Colorado, 2008.*
- 29 Sokolik, I. N., and Toon, O. B.: Direct radiative forcing by anthropogenic airborne
30 mineral aerosols, *Nature*, 381, 681-683, doi:10.1038/381681a0, 1996.
- 31 Sullivan, A. P., and Weber, R. J.: Chemical characterization of the ambient organic aerosol
32 soluble in water: 2. Isolation of acid, neutral, and basic fractions by modified size-exclusion
33 chromatography, *J. Geophys. Res.*, 111, D05315, doi:10.1029/2005JD006485, 2006.
- 34 Sullivan, R. C., and Prather, K. A.: Investigations of the Diurnal Cycle and Mixing State
35 of Oxalic Acid in Individual Particles in Asian Aerosol Outflow, *Environ. Sci. Technol.*, 41,
36 8062-8069, doi:10.1021/es071134g, 2007.
- 37 Sullivan, R. C., Moore, M. J. K., Petters, M. D., Kreidenweis, S. M., Roberts, G. C., and
38 Prather, K. A.: Effect of chemical mixing state on the hygroscopicity and cloud nucleation
39 properties of calcium mineral dust particles, *Atmos. Chem. Phys.*, 9, 3303-3316, 2009.
- 40 Swap, R., Garstang, M., Greco, S., Talbot, R., and Källberg, P.: Saharan dust in the
41 Amazon Basin, *Tellus B*, 44, 133-149, doi:10.1034/j.1600-0889.1992.t01-1-00005.x, 1992.
- 42 Tegen, I., and Lacis, A. A.: Modeling of particle size distribution and its influence on the
43 radiative properties of mineral dust aerosol, *J. Geophys. Res.*, 101, 19237-19244,
44 doi:10.1029/95JD03610, 1996.
- 45 Trochkin, D., Iwasaka, Y., Matsuki, A., Yamada, M., Kim, Y. S., Nagatani, T., Zhang, D.,
46 Shi, G. Y., and Shen, Z.: Mineral aerosol particles collected in Dunhuang, China, and their
47 comparison with chemically modified particles collected over Japan, *J. Geophys. Res.*, 108,
48 48642, doi:10.1029/2002JD003268, 2003.
- 49 Tsyro, S., Simpson, D., Tarrasón, L., Klimont, Z., Kupiainen, K., Pio, C., and Yttri, K. E.:
50 Modeling of elemental carbon over Europe, *J. Geophys. Res.*, 112, D23S19,
51 doi:10.1029/2006JD008164, 2007.

- 1 Ullerstam, M., Vogt, R., Langer, S., and Ljungstrom, E.: The kinetics and mechanism of
2SO₂ oxidation by O₃ on mineral dust, *Phys. Chem. Chem. Phys.*, 4, 4694-4699,
3doi:10.1039/B203529B, 2002.
- 4 Valenzuela, A., Olmo, F. J., Lyamani, H., Granados-Muñoz, M. J., Antón, M., Guerrero-
5Rascado, J. L., Quirantes, A., Toledano, C., Perez-Ramírez, D., and Alados-Arboledas, L.:
6Aerosol transport over the Western Mediterranean basin: Evidence of fine particles to desert
7plumes over Alboran Island, *J. Geophys. Res.*, 119, 14, 028-14, 044,
8doi:10.1002/2014JD022044, 2014.
- 9 Van Dingenen, R., Putaud, J.-P., Martins-Dos Santos, S., and Raes, F., Physical aerosol
10properties and their relation to air mass origin at Monte Cimone (Italy) during the first
11MINATROC campaign, *Atmos. Chem. Phys.*, 5, 2203-2226, doi:10.5194/acp-5-2203-2005,
122005.
- 13 Villani, P., Picard, D., Marchand, N., and Laj, P.: Design and Validation of a 6-Volatility
14Tandem Differential Mobility Analyzer (VTDMA), *Aerosol Sci. Tech.*, 41, 898-906,
15doi:10.1080/02786820701534593, 2007.
- 16 Weinzierl, B., Petzold, A., Esselborn, M., Wirth, M., Rasp, K., Kandler, K., Schütz, L.,
17Koepke, P., and Fiebig, M.: Airborne measurements of dust layer properties, particle size
18distribution and mixing state of Saharan dust during SAMUM 2006, *Tellus B*, 61, 96-117,
19doi:10.1111/j.1600-0889.2008.00392.x, 2009.
- 20 Weinzierl, B., Sauer, D., Esselborn, M., Petzold, A., Veira, A., Rose, M., Mund, S., Wirth,
21M., Ansmann, A., Tesche, M., Gross, S., and Freudenthaler, V.: Microphysical and optical
22properties of dust and tropical biomass burning aerosol layers in the Cape Verde region-an
23overview of the airborne in situ and lidar measurements during SAMUM-2, *Tellus B*, 63, 589-
24618, doi:10.1111/j.1600-0889.2011.00566.x, 2011.
- 25 Wiedensohler, A., Birmili, W., Nowak, A., Sonntag, A., Weinhold, K., Merkel, M.,
26Wehner, B., Tuch, T., Pfeifer, S., Fiebig, M., Fjåraa, A. M., Asmi, E., Sellegri, K., Depuy, R.,
27Venzac, H., Villani, P., Laj, P., Aalto, P., Ogren, J. A., Swietlicki, E., Williams, P., Roldin, P.,
28Quincey, P., Hüglin, C., Fierz-Schmidhauser, R., Gysel, M., Weingartner, E., Riccobono, F.,
29Santos, S., Gruning, C., Faloon, K., Beddows, D., Harrison, R., Monahan, C., Jennings, S. G.,
30O'Dowd, C. D., Marinoni, A., Horn, H. G., Keck, L., Jiang, J., Scheckman, J., McMurry, P.
31H., Deng, Z., Zhao, C. S., Moerman, M., Henzing, B., de Leeuw, G., Löschau, G., and
32Bastian, S.: Mobility particle size spectrometers: harmonization of technical standards and
33data structure to facilitate high quality long-term observations of atmospheric particle number
34size distributions, *Atmos. Meas. Tech.*, 5, 657-685, doi:10.5194/amt-5-657-2012, 2012.
- 35 Zhou, M., Okada, K., Qian, F., Wu, P. M., Su, L., Casareto, B. E., and Shimohara, T.:
36Characteristics of dust-storm particles and their long-range transport from China to Japan -
37case studies in April 1993, *Atmos. Res.*, 40, 19-31, doi:10.1016/0169-8095(95)00023-2, 1996.
- 38